Fig. 60

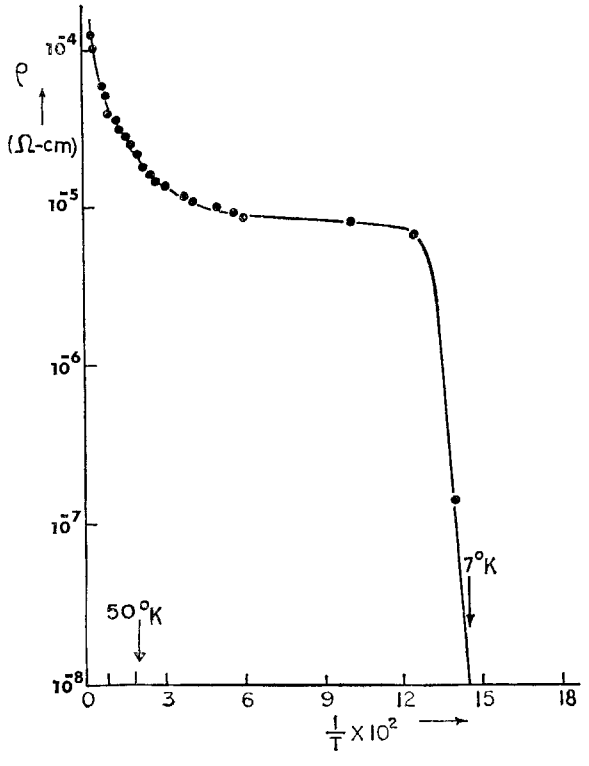

(*a*)

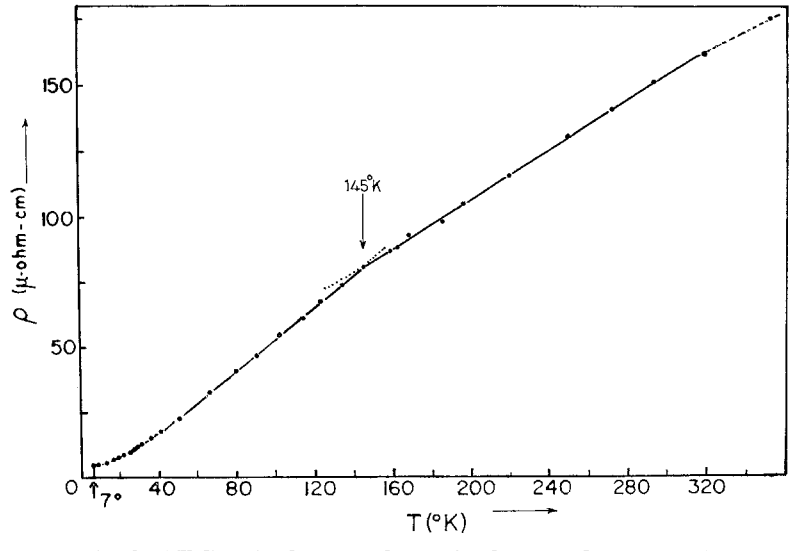

(*b*)

(*a*) ρ versus $1/T$ for $NbSe_2$ single crystals. (Kershaw *et al.* 1967.) (*b*) ρ versus T for $NbSe_2$ single crystals. (Lee *et al.* 1969.)

Electrical data on single crystals of these materials are very sparse. The resistivity plot of fig. 60 (*a*) is a single crystal measurement for $NbSe_2$. It indicates clearly the superconducting break. The temperature coefficient of resistance for these metals is $\sim 4 \times 10^{-3}$/°C and in this they are very comparable to, say, silver. Further data, obtained by Brixner on powdered compacts, are given below:

Brixner (1962)	$\rho_{300°K}$	$\rho_{77°K}$	S	κ_{th}
$NbSe_2$	$3{\cdot}5 \times 10^{-4}$	$1{\cdot}8 \times 10^{-4}$	-12	0·021
$TaSe_2$	$4{\cdot}0 \times 10^{-4}$	$3{\cdot}1 \times 10^{-4}$	-13	0·017
	ohm-cm		μV/°C (compare VSe_2, +30)	W/°C/cm

It is not known what happens at high temperatures, where the considerations of Fivaz's theory of electron–phonon interaction may become important (see p. 268). Examination of the free-carrier rise at raised temperatures is to be attempted.

Fig. 61

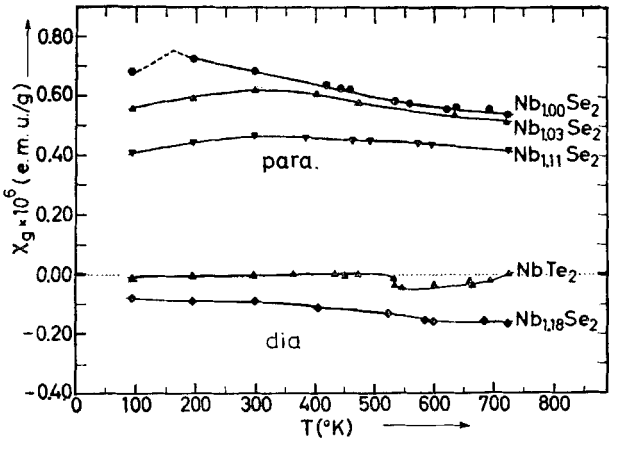

Magnetic susceptibility of $Nb_{1+x}Se_2$ and $NbTe_2$.
(Selte and Kjekshus 1965.)

The magnetic properties of these compounds are very interesting. From the preliminary susceptibility measurements on $NbSe_2$ and $TaSe_2$ (figs. 61 to 64) it seems that these compounds show band antiferromagnetism

below 160°K and 130°K respectively (Theory—see Herring 1966, Rice *et al.* 1969). As with chromium ($T_N = 475$°K) the conductivity is not discontinuous at T_N, apart from a local anomaly, see fig. 60 (*b*); (see Arko *et al.* 1968, and Meaden and Sze 1969 for the case of chromium). This contrasts with the behaviour of several other narrow band metallic compounds. NiS for example (two free electrons per formula unit) shows a factor increase of 50 in the resistivity on cooling through the Néel point (268°K), and semiconducting properties appear. It is clear that in the NbS_2 family band behaviour is better established than it is in say NiS, or VO_2 ($T_d = 341$°K, $\rho_{400°K} \sim 1 \times 10^{-3}\,\Omega$-cm), where electron–electron and electron–phonon interactions lead to low temperature semiconducting phases. The plasma edge occurs at 8000 cm^{-1} in metallic VO_2 (Barker *et al.* 1966) as against 10 000 cm^{-1} in NbS_2 and 9000 cm^{-1} in $NbSe_2$. Many estimates of the effective mass in metallic VO_2 have been made ranging up to $40\,m_e$, but the typical values quoted seem notably higher than the suggested values for $NbSe_2$, etc., viz. $1 < m^*/m_e < 3$†.

Fig. 62

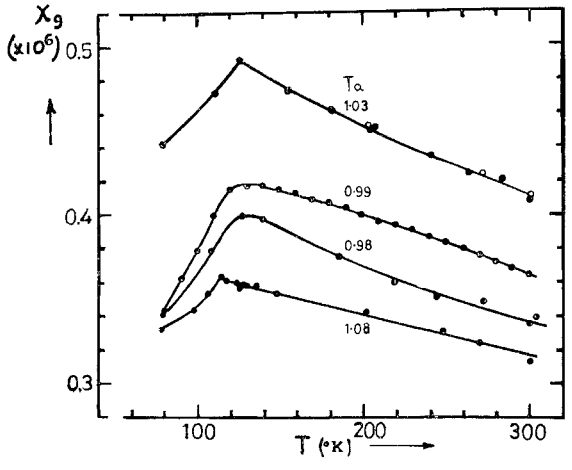

Magnetic susceptibility of trigonal prism $Ta_{1+x}Se_2$. (Quinn *et al.* 1966.)

Returning to the details of figs. 61 to 64 it is found that application of the Curie–Weiss expression $\chi = C/T - \theta_p$ to the susceptibility above T_N gives very odd results. θ_p values of *ca.* -2100°K and -2600°K are found for $NbSe_2$ and $TaSe_2$ respectively, with n_{eff} values of $2{\cdot}4\,\mu_B$. The peak susceptibilities are very similar, at 180×10^{-6} e.m.u. units/mole. This

† It has not proved possible to obtain a reliable value of m^* for NbS_2, etc. from an analysis of the wavelength dependence of the free-carrier absorption, since the latter rises very quickly to very high values, and not with the classical λ^2 form. In the degenerate layer semiconductor Bi_2Se_3 Gobrecht *et al.* (1966) obtained a dependence as $\lambda^{3{\cdot}5}$, over the range 6 to 12 μ.

Fig. 63

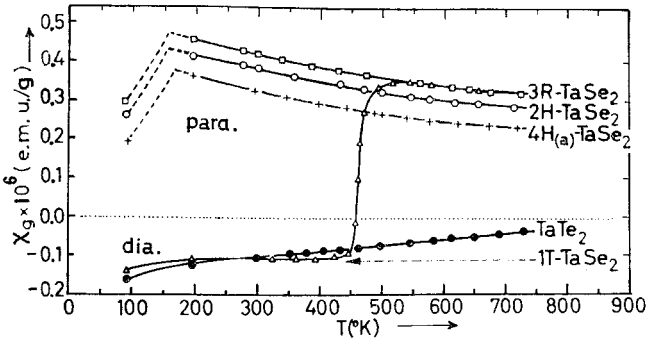

Magnetic susceptibility of the various polytypes of $TaSe_2$; also $TaTe_2$. (Bjerkelund and Kjekshus 1967.)

Fig. 64

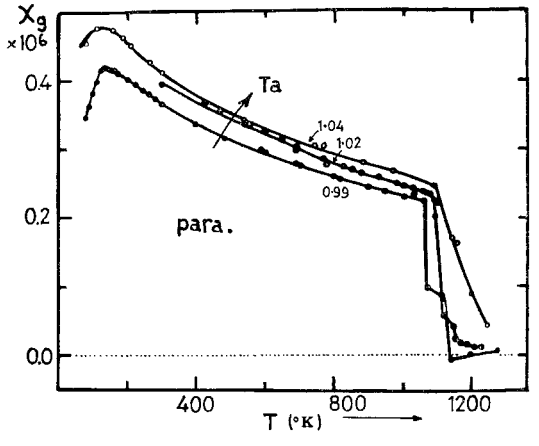

High temperature susceptibility of several $TaSe_2$ specimens. (Quinn *et al.* 1966.)

combination of high θ_p and low χ is typical of materials far removed from 'ionic' localized d state behaviour. The peak susceptibility value of VSe_2 ($T_N \sim 230°K$—Røst *et al.* 1964) likewise is only 340×10^{-6} e.m.u. units/mole. These values should be compared with the very much higher susceptibility for the more ionic α-$TiCl_3$ ($T_N = 220°K$) of about 1000×10^{-6}/mole (see § 9.3). Magnetism in all the above compounds is the product of a single electron. The peak susceptibility in Cr metal is down again to 187×10^{-6} e.m.u. units/mole. Values in this latter range are of the order found for straight Pauli paramagnetism in metals, e.g.

Pt 214×10^{-6}, Mg 134×10^{-6}, $NiTe_2$ 88×10^{-6} e.m.u./mole.

It is not known what happens to the lattice parameters of the $NbSe_2$ family below T_N (there is a 2% volume *increase* in NiS). A neutron diffraction study is awaited. What is known is that the susceptibility depends on the stacking polytypes being used and is also markedly dependent on the stoichiometry of the sample. Metal excess quickly reduces the susceptibility. It is also known to lead to a rapid decrease in the superconducting transition temperature (Van Maaren and Schaeffer 1966, 1967). (This is not so in the superconducting series $PdTe_2 \leftrightarrow PdTe$—Kjekshus and

Table 10. Superconducting transition temperatures of the group V dichalcogenides

Material	T_s°K	Reference
2H–NbS_2	6·3	Van Maaren and Schaeffer (1966)
3R–NbS_2	5·5	
2H–$NbSe_2$	7·0	Revolinsky *et al.* (1965)
4H–$NbSe_2$	6·3	
$NbTe_2$	0·74	Van Maaren and Schaeffer (1967)
1T–TaS_2	0·8	
2H–$TaSe_2$	0·15	
3R–$TaSe_2$	0·22	

T_s not above 0·05°K in $V_{1+x}Se_2$, $V_{1+x}Te_2$ and $TaTe_2$.

Pearson 1965.) What the magnetic properties of these compounds are like close to the superconducting transition should provide an interesting study†. The superconducting temperatures of the group V specimens so far examined are given in table 10. The superconducting temperatures of the tantalum compounds are markedly lower than those of niobium—a not uncommon feature of 5d materials. The properties of the unusual 1T polytypes and of the ditellurides are discussed in § 8.

For the trigonal prism *metals* it is likely that the Fermi surface, if formed from the d_{z^2} orbital as suggested above, is of the form shown in

Fig. 65

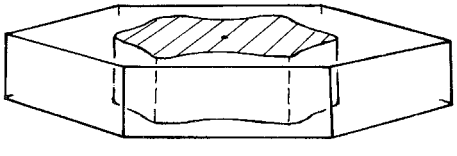

Postulated form of the Fermi surface for 2H–NbS_2, etc.

† Such behaviour is not entirely unknown, La/Gd alloys showing some coexistence of magnetic and superconducting conditions (cf. Rado and Suhl, Vol. 2B, p. 209).

fig. 65. Its 'cylindrical' shape expresses the fact that, as in MoS_2, there is likely to be a factor of about 10^2–10^3 difference in the carrier mobilities $\parallel$ and $\perp$ to c. It is hoped to confirm this shape by de Haas van Alphen measurements, but the crystals at present available are inadequate in size and perfection to make a proper study. Such measurements have recently been performed on the layer material Bi_2Te_3 (Mallinson *et al.* 1969), and on the d band metal ReO_3 (Marcus 1968).

7.3.2. *Group V materials as superconductors*

An intriguing possibility that this family of compounds offers is of manipulating the superconducting transition temperature over fairly wide limits via substitutional doping, e.g. (Nb/Mo)Se_2. V/VI substitution occurs very readily. Figure 66 shows the steady variation of lattice parameters in the system (Ta/W)Se_2. We see that in the high tantalum range the structure obtained is of the 3R–MoS_2 polytype common to both group V and group VI (see fig. 3). Figure 67 and table 11 show how σ and S vary in this system. The carrier type is seen to change from n to p just above the half-filled band concentration (viz. 55 at. % W). This suggests a tight-binding sinusoidal form to the E versus k bands. B.C.S. theory of superconductivity gives for the transition temperature T_S, in the phonon mechanism:

$$T_S = 1{\cdot}14\,\Theta_D \,.\, \exp\,[(-1/N(O)V)],$$

Fig. 66

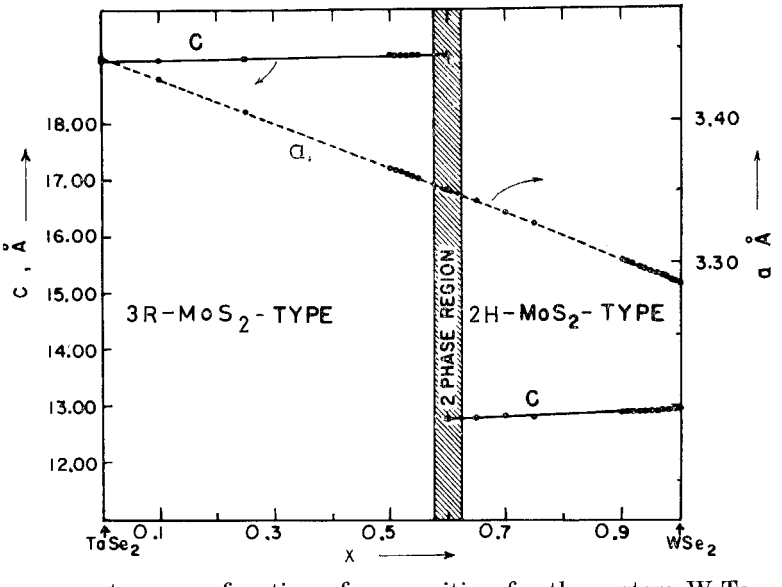

Lattice parameters as a function of composition for the system $W_xTa_{1-x}Se_2$. (Brixner 1963.)

Table 11. Electrical data on (W/Ta)Se_2 for plot of fig. 67. (Brixner 1963)

x	ρ m . ohm-cm 25°C	ρ m . ohm-cm −196°C	S μv/°C 25°C	
0 ($TaSe_2$)	0·40	0·31	−10	
0·10	0·60	0·45	−9	
0·25	0·55	0·42	−6	
0·50	0·72	0·59	−2	n
0·51	0·82	0·53	−1·5	
0·52	0·83	0·51	−1·0	
0·53	0·75	0·54	−0·6	
0·54	0·79	0·57	−0·2	
0·55	0·80	0·58	+0·5	
0·60	0·95	0·80	+2·0	
0·65	0·92	0·83	+6	
0·70	0·88	0·80	+10	
0·75	1·01	0·93	+14	
0·90	1·10	0·95	+33	
0·91	1·10	0·96	+36	
0·92	1·15	0·97	+39	
0·93	1·23	0·96	+44	p
0·94	1·40	1·09	+48	
0·95	1·49	1·18	+56	
0·96	1·70	1·58	+65	
0·97	1·90	1·83	+75	
0·975	3·50	2·90	+90	
0·98	4·51	4·00	+100	
0·985	5·71	6·02	+110	
0·99	6·92	7·21	+120	
1 (WSe_2)	719	$1·2 \times 10^5$	+700	

where $N(O)$ is the density of states at the Fermi energy (0°K), and V is the effective attractive electron–electron interaction. For MoS_2 Θ_D is 210 °K (Salaam 1960), and this is likely to be fairly constant throughout a system like (Nb/Mo)S_2 (N.B. for Nb metal, T_S 9·2 °K, $\Theta_D = 250$ °K). Recently there has been considerable investigation into the superconductivity ($T_S \lesssim \frac{1}{4}$°K) found in the semiconductors $SrTiO_2$ (Koonce *et al.* 1967), GeTe and SnTe (Allen and Cohen 1969), when prepared in the degenerate condition. Cohen and Koonce (1966) and Koonce and Cohen (1969) have given expressions for the attractive potential V in terms of the intra-valley and inter-valley phonon couplings. T_S is large when these phonon couplings are large, as may well be the case in a layer compound (see Fivaz and Mooser 1967, and p. 268). Also the density of states $N(O) \sim m^* . n^{1/3}$ will be large in NbS_2. Actually too many carriers can screen out the superconductive attractive potential, and in $SrTiO_3$ T_S passes through a maximum at $n_c = 8 \times 10^{19}/cm^3$. Hence our interest in the mixed systems like (Nb/Mo)S_2, and possibly (Mo/Tc)S_2, though this system is not fully

miscible. Further, in the latter system the carriers are in the d/p rather than in the d_{z^2} band.

Fig. 67

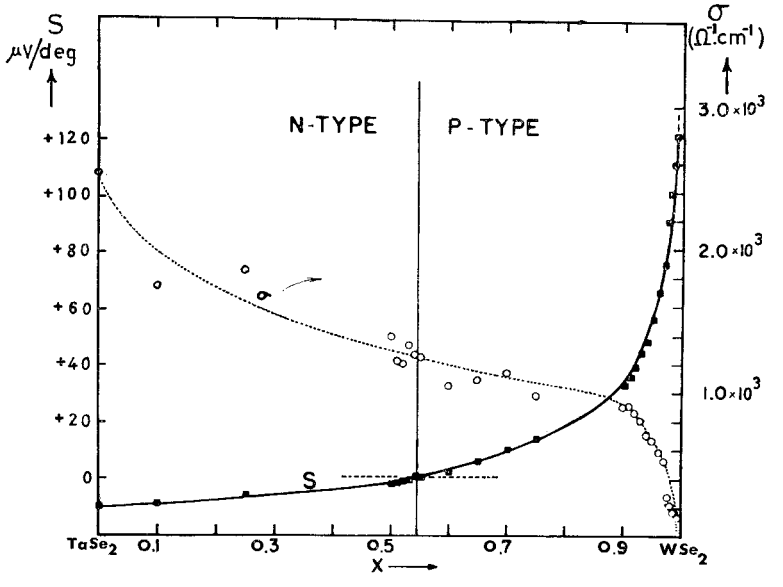

Variation of σ and S through the system $W_xTa_{1-x}Se_2$. (Brixner 1963.)

Any superconductivity arising in compositions not too far removed from MoS_2 could be of great interest in efforts to obtain very high transition temperatures. The very stable excitons formed in connection with the d/p band (see p. 245) could lead to the occurrence of the recently proposed excitonic mechanism for superconductivity (see Ginzburg 1968). The mechanism is one of direct interaction in the Bose–Einstein gas of excitons, rather than of electron–electron interaction through phonon mediation. Since the Θ value in the B.C.S. equation is now an electronic rather than a lattice temperature, T_S stands the possibility of being raised at least above the liquid hydrogen barrier (20·4 °K). The quasi two-dimensional character of these layer materials is also thought likely to contribute to this end.

It is not expected that any optical effects will be noted in the visible range when these materials are in their superconducting state (Tinkham 1966), but the crystals are well suited to far infra-red work. There the superconducting energy gap for NbS_2 should lie at about 20 cm^{-1} (i.e. $\sim 4kT_S$). Alternatively the gap could be studied quite easily using the tunnelling technique. In such experiments the effects of crystal thickness on T_S could be readily ascertained. It has been found for many systems that T_S increases markedly as the specimen thickness is reduced. As with lamellar intercalated graphites (Salzano and Strongin 1967) it is presumed

that the crystals become superconducting both || and ⊥ to c at the same T_S. Anisotropy is, however, reported in critical current measurements (Spiering *et al.* 1966). It has already been noted that T_S changes with the different stacking polytypes; in these cases the phonon spectrum may be more significantly altered than is the electronic band structure. It is also likely that the phonon spectrum is strongly modified in very thin specimens.

Moreover, Kogan and Tavger (1966) predict that for thicknesses $\lesssim 100$ Å, when the electron states lie virtually in two-dimensional sheets in the Brillouin zone, superconductivity could arise even in *non*-degenerate semiconductors ($n \sim 10^{17}$/cm^3). Such a material could be obtained by very light doping of MoS_2 with niobium. Moreover, crystal thicknesses of this order are accessible using layer crystals.

7.3.3. *Doped materials, intercalates and exciton screening*

The main fall in resistivity in a V/VI system like, say, (W/Ta)Se_2, comes of course close to the group VI end, when the small gap semiconductor (here WSe_2) gives way first to highly degenerate semiconducting behaviour ($\lesssim 1\%$ Ta), and then to complete metallicity. These changes are given in table 12 and figs. 68 and 69. The effective free-carrier yield (holes) per added Ta atom is only one-fifth at doping level $x = 0{\cdot}005$ (i.e. $\frac{1}{2}$ at. %), but rises to approximately unity with 2% doping. At this level the Seebeck coefficient has dropped below 200 μv/°c. Hicks (1964) obtained quite good fits to his Seebeck data (see fig. 68 (*c*)) over the doping range 1 to 5% using Johnstone's curves (1956) for scattering in degenerate semiconductors. At 5% doping the scattering is principally as from ion centres ($\mu_H \propto T^{-0{\cdot}5}$), and the fit leads to the deduction that $m_h^* \sim m_0$. The intrinsic zero doping data were only fitted with the additional assumptions that $\mu_e \sim \mu_h$ and $m_e^* \sim m_h^*$, but it is suspected that this fit was attempted using $E_g = 1{\cdot}7$ ev, corresponding to the excitonic energy gap ($\sigma \rightarrow$ d/p, see fig. 27), rather than the d–d gap which is about 0·1 ev. Fivaz and Mooser (1967), or Revolinsky and Beerntsen's (1964) data show that the smaller gap is the carrier determining gap in intrinsic material at least until 600°c (see fig. 53, and p. 269).

Table 12. Electrical data on tantalum doped WSe_2. (Hicks 1964)

Compound	x	ρ *m.* ohm-cm	R_H cm^3/coul	n cm^{-3}	μ cm^2/v-sec	$\frac{n_e}{n_{at}}$
$W_{1-x}Ta_xSe_2$	0	780	78	$8{\cdot}0 \times 10^{16}$	99	—
	0·005	30·2	$3{\cdot}9 \times 10^{-1}$	$1{\cdot}6 \times 10^{19}$	12·9	0·2
	0·01	11·7	$7{\cdot}4 \times 10^{-2}$	$8{\cdot}4 \times 10^{19}$	6·3	0·6
	0·02	4·3	$2{\cdot}5 \times 10^{-2}$	$2{\cdot}5 \times 10^{20}$	5·8	0·9
	0·03	3·2	$1{\cdot}8 \times 10^{-2}$	$3{\cdot}5 \times 10^{20}$	5·6	0·8
	0·04	—	$1{\cdot}5 \times 10^{-2}$	$4{\cdot}2 \times 10^{20}$	—	—
	0·05	2·5	$9{\cdot}4 \times 10^{-3}$	$6{\cdot}6 \times 10^{20}$	3·8	0·9

Fig. 68

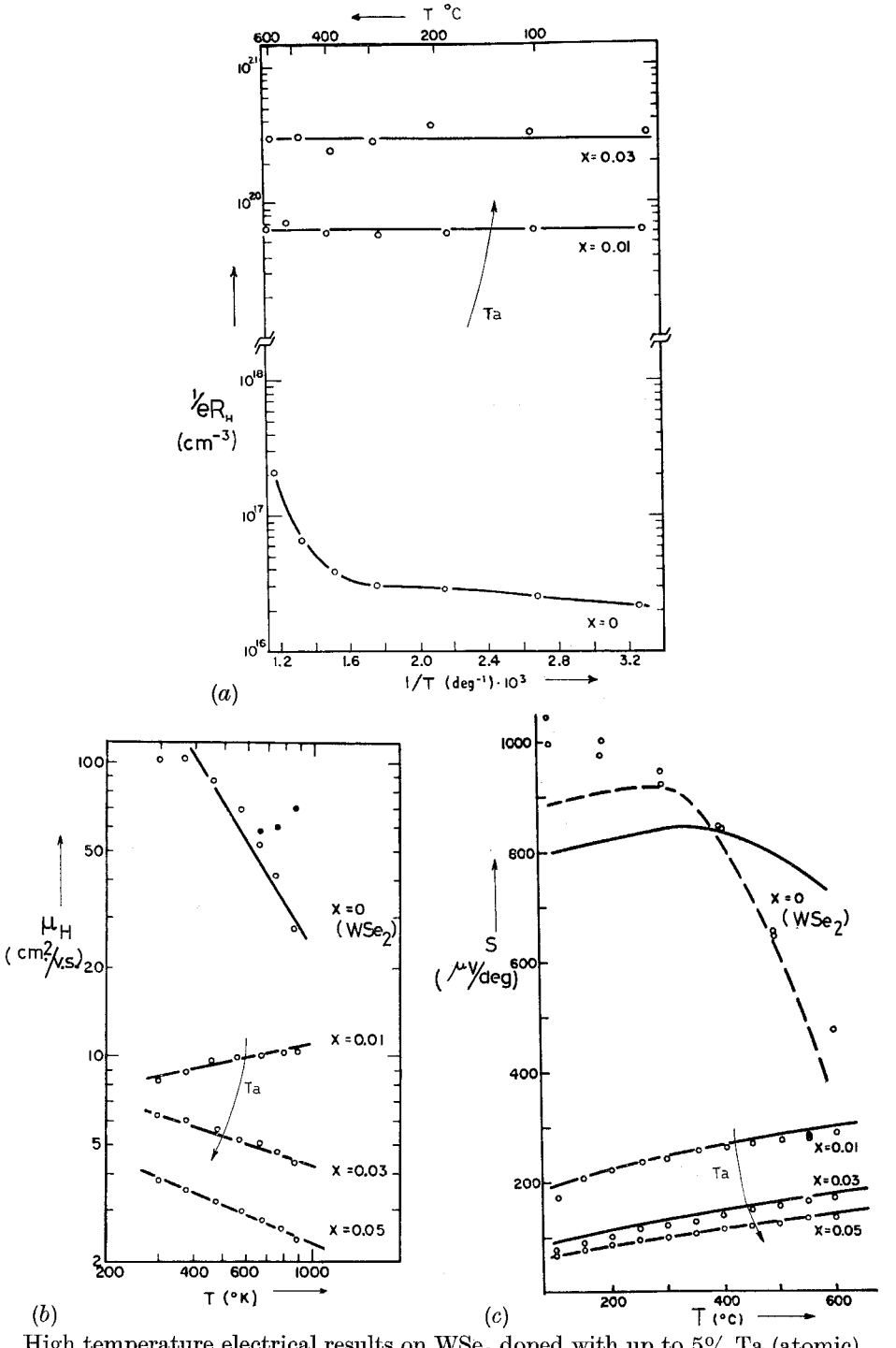

High temperature electrical results on WSe_2 doped with up to 5% Ta (atomic). (*a*) Number of carriers, (*b*) Hall mobility, (*c*) Seebeck coefficient. (Hicks 1964.)

Increase of the carrier concentration in a group VI semiconductor through group V doping has an interesting effect on the excitons A and B. The effective two-body electron–'hole' exciton interaction in the carrier sea is:

$$V(r) = -\frac{1}{\epsilon(r)} \cdot \frac{e^2}{r} \cdot \exp(-qr).$$

The exponential screening term arises from the free carriers which are able to respond and to 'dissolve' the bound exciton state. The screening parameter q will depend on the density of these free carriers and their mobility, and also on the expectation radius of the exciton, which is governed among other things by its effective mass (a function of the bands in which its one-electron state components lie).

Fig. 69

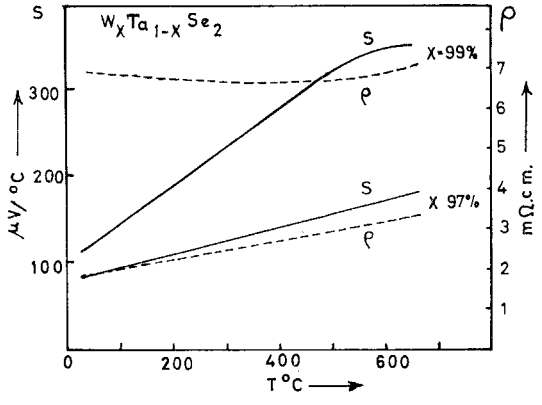

High temperature measurements of ρ, and S for (*a*) 1% (atomic) Ta in WSe_2, (*b*) 3%. (Brixner 1963.)

The course of free-carrier screening may be followed through by controlled doping. The exciton binding energy in germanium is very small ($\sim 10^{-3}$ ev) and the peak is accordingly very temperature dependent (see fig. 39, Phillips 1966). Asnin and Rogachev (1967) have recently succeeded in progressively screening out this feature from the transmission spectrum by using doping concentrations from 10^{13} up to $10^{17}/cm^3$. Their results are shown in fig. 70. Because of the much larger exciton binding energy for MoS_2 ($\sim 0{\cdot}05$ ev) and the smaller radius (20 Å as against 200 Å) it has been found possible to parallel their experiment at much more convenient doping levels. As seen in table 12, doping WSe_2 with 1% Nb, say, will increase the conductivity by 10^2 or more whilst the carrier concentration changes from 10^{17} to $10^{20}/cm^3$. Figure 71 shows the spectra obtained for such systems. The disappearance of the excitons is not due to poor crystal quality, as is seen from electron micrographs and also from the results on other mixed

Fig. 70

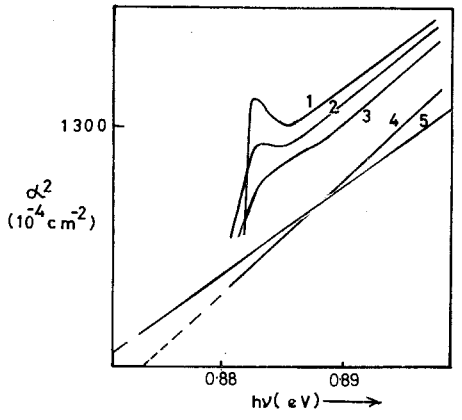

Effect on the exciton in germanium of arsenic doping. (1) 3×10^{13}, (2) 2×10^{15}, (3) 1×10^{16}, (4) $2 \times 10^{1 \cdot 7}$, (5) $1 \cdot 5 \times 10^{18}$/cm^3. (Asnin and Rogachev 1967.)

Fig. 71

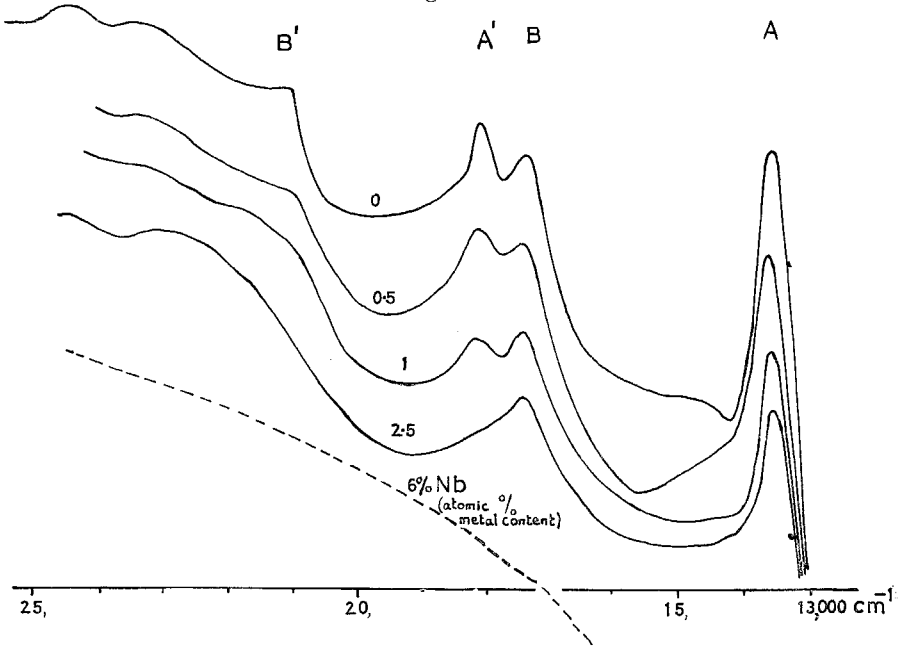

Effect on the excitons in WSe_2 of niobium doping (curves staggered—common level of absorption at energies greater than B').

systems such as (W/Mo)Se_2 or Mo(S/Se)$_2$, where the excitons still show strongly (see p. 245). It could be, though, that the doping concentrations used in the VI/V system are high enough for exciton–electron *collisions* to

be very important. The free carriers, however, are *not* introduced into a band occupied by either the electron or the hole of the exciton.

Finally it should be noted that even in NbS_2 itself there is some trace of peaking in the exciton energy range (see fig. 22 (*h*)). It remains to be seen what happens at liquid helium temperatures (actually at 4°K, NbS_2 would be a superconductor—see p. 277). The most surprising thing in these compounds is that any excitonic interaction persists at all in the presence of such high carrier concentrations—even though these carriers are not very mobile. Recently Mahan has published two theoretical papers (1967 a, b) discussing such remanent excitonic interaction in highly degenerate semiconductors and poor metals.

A further very interesting means of doping these layer structures is by the process known as 'intercalation'. In intercalation atoms of an additional element are taken up into the vacant van der Waal's sites. The take-up of the alkali metals from liquid ammonia solution in particular has been studied (Rudorff 1965). Intercalation compounds of graphite, like C_8K, have recently been shown to be superconducting (Salzano and Strongin 1967). It seems that in such compounds the alkali metal donates its outer electron into an existing energy band of the matrix. In this the intercalates closely resemble the 'bronzes' of which the tungsten bronzes, A_xWO_3, are the simplest and best known (e.g. Sienko 1962). The tungsten bronzes are based on a cubic cell, body-centred by tungsten, face-centred by the oxygens, and accommodating any added alkali metal atoms at cube corner sites. The tungsten t_{2g} orbitals are not involved in the σ bonding of the WO_3 octahedra, and go to form an empty non-bonding band. It is this band which accepts any electrons donated by added alkali atoms, so yielding a situation akin to that for the metallic compound ReO_3 (Feinleib *et al.* 1968). This sequence is very much like that of, say, $TiSe_2$, intercalated $TiSe_2$, and VSe_2. Alkali metal intercalation by TiS_2 (group IV) or MoS_2 (group VI) is known to produce a metallic product, as witnessed

Table 13. Properties of intercalated TiS_2, 'VS_2' and 'CrS_2'. (Rudorff 1965)

Compound	$Na_{0\cdot8}TiS_2$	$NaVS_2$	$NaCrS_2$
Colour	Black	Black	Orange
Lattice constants (Å)			
a	$3\cdot5_3$	$3\cdot5_7$	$3\cdot5_3$
c	$20\cdot0_4$	$19\cdot6_5$	$19\cdot4_9$
Magnetic moment B.M.			
μ_{eff} ($T=293$°K)	0·61	2·1	3·7
$\mu_{\text{theoretical}}$	1·73	2·83	3·87
Specific resistivity Ω-cm	Small	0·2	$>10^8$
Reaction with water	H_2 liberated	Slow hydrolysis	Stable

by the low resistivity and Pauli paramagnetism (Rudorff 1965). Intercalation tends to run to a product A_xTX_2, where x is fixed for a given compound TX_2, but is usually less than 1, e.g. for potassium in WS_2, MoS_2, ReS_2, $x=0{\cdot}5$, $0{\cdot}6$ and $0{\cdot}8$ respectively. The a and particularly the c parameters are increased by such intercalation, but the c expansion is noted to be smaller for larger x, e.g. 2·01, 1·95 and 1·65 Å in the above-mentioned cases. This could mark an increasing tendency towards ionic behaviour. Certainly such a tendency is very marked through the intercalated products of TiS_2, 'VS_2', 'CrS_2' as table 13 from Rudorff 1965) shows. Indeed, $NaCrS_2$ has optical and magnetic properties which indicate the presence of Cr^{3+} ions (Holt and Wold 1967, Bongers *et al.* 1968). This compound is more like a standard perovskite or spinel than an intercalation product. In fact $CrS_2/Se_2/Te_2$ do not exist (as either layer compounds or pyrites) even under high pressures and temperatures—see p. 321. The progressive increase in ionicity and the breakdown of band behaviour through the series $NaTiS_2$, $NaVS_2$, $NaCrS_2$ is very similar to that in a perovskite series such as $LaTiO_3$, $LaVO_3$, $LaCrO_3$, $LaMnO_3$. Collective to localized transitions in such series have been much investigated lately (e.g. Goodenough 1966, 1967 a, b). Returning to the non-stoichiometric 'bronzes' and 'intercalates' these too are of interest as regards the metal–insulator transition. It is well known (Mott 1967, Shanks *et al.* 1962) that in some cases metallic type conductivity does not appear until the alkali content is quite substantial. The intercalates of MoS_2, etc., have yet to be investigated from this aspect. If progressive intercalation can be secured it might be possible to observe the steady disappearance of the A and B excitons due to screening. Also of interest are the superconducting properties of the intercalates. Several of the 'bronzes' are known to be superconductors (Sleight *et al.* 1969), as of course is degenerate $SrTiO_3$ (Koonce *et al.* 1967). The intriguing possibilities for superconductivity in the TX_2 layer dichalcogenides have been mentioned already in § 7.3.2.

7.4. *The Group VIII Layer Materials*

The layer tellurides of group VIIIb, $CoTe_2$, $RhTe_2$, and $IrTe_2$, are all very metallic. The metallic character seems better established as compared with that of the non-layered selenides. Thus $CoTe_2$ (Haraldsen *et al.* 1956) does not show the cooperative magnetism of CoS_2 or $CoSe_2$ (see § 9.1), and layered $RhTe_2$ is not a superconductor, unlike the pyrite forms of $RhSe_2$ and $RhTe_2$. $IrTe_2$ contrasts strongly with orthorhombic $IrSe_2$, which is a semiconductor (see Hulliger 1964). These layer tellurides like those of Group VIIIc (viz. $NiTe_2$, $PdTe_2$, $PtTe_2$) all have a very small c/a parameter (see fig. 14 and table 2). Resistivities of $\sim 10^{-5}\,\Omega$-cm for $PtTe_2$, etc. again contrast strongly with the semiconductivity obtained in PtS_2 and $PtSe_2$. Semiconductivity was to be expected for group VIIIc in the light of the band diagram of fig. 26(*b*). The very small band gap observed for $PtSe_2$ ($\sim 0{\cdot}1$ ev, Hulliger 1965) would indicate that for all

six tellurides the non-bonding d band now overlaps the σ^* conduction band. The degree of overlap must be just right to produce superconductivity in $PdTe_2$ (T_S 1·8°K, Kjekshus and Pearson 1965), but not in either $NiTe_2$ or $PtTe_2$ (Guggenheim *et al.* 1966). The c/a contraction is to be expected as the non-bonding orbitals, which have the geometry shown in fig. 25, become highly occupied. In fact it is likely that there is heavy mixing of all the states in these tellurides. c/a has its minimum value of 1·27 in $PdTe_2$, as against 1·30 in $PtTe_2$ and 1·37 in $NiTe_2$. $PdTe_2$ should also be compared with $ZrTe_2$ from group IV, where the d band is empty.

	a	c	$\frac{2r_{at.}}{d_{M-M}}$	c/a
$ZrTe_2$	3·950	6·630 Å	81%	1·678 (c/a ideal = 1·633)
$PdTe_2$	4·037	5·126 Å	68%	1·270

Further details of the electrical and structural properties for the whole of group VIII are given later in § 9.

§ 8. The Optical and Electrical Properties of the *Distorted* Layer Compounds of Groups V, VI and VII

8.1

The compounds with which we are concerned here are:

(1) Group VII. 3 'non-bonding' electrons, ReS_2, $ReSe_2$, ($ReTe_2$), TcS_2, $TcSe_2$ ($TcTe_2$).

(2) Group VI. 2 'non-bonding' electrons, WTe_2, β-$MoTe_2$.

(3) Group V. 1 'non-bonding' electron, $TaTe_2$, $NbTe_2$.

These TX_2 layer compounds are all based on the octahedral sandwich but with the metal atoms displaced from the coordination unit centres. This causes the X atom sheets to buckle somewhat. The detailed crystal structures have been given in figs. 4, 5 and 6. The pattern of metal atom displacements changes from group to group with the number of spare electrons not involved in σ bonding. The resulting metal–metal interactions make for the establishment of filled sub-bands, i.e. we have homopolar metal–metal bonding. Figure 25 shows the geometry of the orbitals involved. ReS_2 with three non-bonding electrons would be a metal in either trigonal prism or octahedral coordination *if* regular (see fig. 26 (*b*)). Actually the material is a semiconductor showing a sharp excitonic feature on the absorption edge (see fig. 22 (*j*)). The distortion is particularly strong

in this case. The Re atoms cluster into units of 4, with the shortest Re–Re distance less than that in the h.c.p. metal itself†. Figure 72 and table 14 compare the structures for the three groups together, and also with the distorted rutile VO_2 (see fig. 73). In VO_2 (below T_d) we have discrete pairs of vanadium atoms, whilst in the layer compounds we have strands of linked atoms.

Table 14. Comparison of the distortions in $NbTe_2$, WTe_2, $ReSe_2$ and VO_2

	$NbTe_2$	WTe_2	$ReSe_2$	VO_2
$\frac{\text{Shortest M–M}}{\text{Average M–M}}$	$\frac{3{\cdot}33}{3{\cdot}83}=0{\cdot}87$	$\frac{2{\cdot}86}{3{\cdot}58}=0{\cdot}80$	$\frac{2{\cdot}65}{3{\cdot}35}=0{\cdot}79$	$\frac{2{\cdot}65}{2{\cdot}88}=0{\cdot}92$ ‖c
$\frac{\text{Shortest M–M}}{\text{Longest M–M}}$	$\frac{3{\cdot}33}{4{\cdot}51}=0{\cdot}74$	$\frac{2{\cdot}86}{4{\cdot}38}=0{\cdot}65$	$\frac{2{\cdot}65}{4{\cdot}13}=0{\cdot}64$	$\frac{2{\cdot}65}{3{\cdot}12}=0{\cdot}85$
$\frac{\text{Shortest M–M}}{\text{Shortest in metal}}$	$\frac{3{\cdot}33}{2{\cdot}86}=1{\cdot}165$	$\frac{2{\cdot}86}{2{\cdot}74}=1{\cdot}045$	$\frac{2{\cdot}65}{2{\cdot}75}=0{\cdot}965$	$\frac{2{\cdot}65}{2{\cdot}63}=1{\cdot}009$
Area of sheet in bonding region	58%	36%	44% (strips) or 20% (diamonds)	—
$\frac{\text{Shortest M–X}}{\text{Longest M–X}}$	$\frac{2{\cdot}690}{2{\cdot}908}=0{\cdot}925$	$\frac{2{\cdot}708}{2{\cdot}820}=0{\cdot}962$	$\frac{2{\cdot}382}{2{\cdot}665}=0{\cdot}893$	$\frac{1{\cdot}86}{2{\cdot}05}=0{\cdot}906$

Electrical and optical polarization measurements have as yet failed to reveal any anisotropy *in* the layers, but this may be due to twinned domain formation (see later). The energy derived from the metal–metal bonding and from a number of shortened T–X distances must more than compensate for the increased length of the other T–X bonds in the coordination units. The energy difference between a distorted and regular phase is clearly small. $MoTe_2$ moves from the regular α to the distorted β form above 900°C, whilst VO_2 becomes regular above 68°C. Perhaps the best indication of the strength of the metal–metal bonding comes from the ratio of the shortest and longest M–X distances since these bonds are of prime energetic importance. This places $ReS_2 > VO_2 > NbTe_2 > WTe_2$ (see table 14).

This type of metal sub-lattice distortion is fairly common among oxides, halides and chalcogenides possessing narrow d bands. When the room temperature carrier mobility for a band drops below about 10 cm^2/v-sec,

† This is typical of many rhenium compounds—see Canterford and Colton (1968) for halide examples. $ReTe_2$ has a very complex distorted layer structure —see Sorrell (1968). It is reported to be a p type semiconductor (see Johnson *et al.* 1965).

the entropy term causes delocalization to be unfavourable (Mott 1969). Several mechanisms are known which then tend to produce filled band insulators. In several cases, a sharp semiconductor↔metal transition is obtained at temperatures easily accessible to experiment. In VO_2 a 10^5 drop in ρ from 10 to 10^{-4} Ω-cm, occurs on warming at 68°C (Ladd and Paul 1969). The VO_2-type distortion transition can be described in terms of electron–phonon interaction. It is a 'fixation' of the small polaron effect (Appel 1969) when the structure and number of electrons are favourable to permanent distortion. The distortion causes a previously degenerate band to split into sub-bands. If the distortion is severe as in VO_2 or ReS_2 the splitting can separate the bands throughout the zone so that a semiconductor results. Neither a structure analysis nor electrical measurements have been made on TcS_2 and $TcSe_2$, but from the absence of the exciton peaks on the direct edge, as compared with ReS_2 and $ReSe_2$ (fig. 22 (*j*, *k*)) it would seem that the distortion is less severe. The transition temperatures, T_d, etc. are known to be very sensitive to the degree of band overlap (cf. NbO_2, $T_d \sim 1000$°C as compared with VO_2, $T_d = 68$°C—see Adler 1968).

Fig. 72

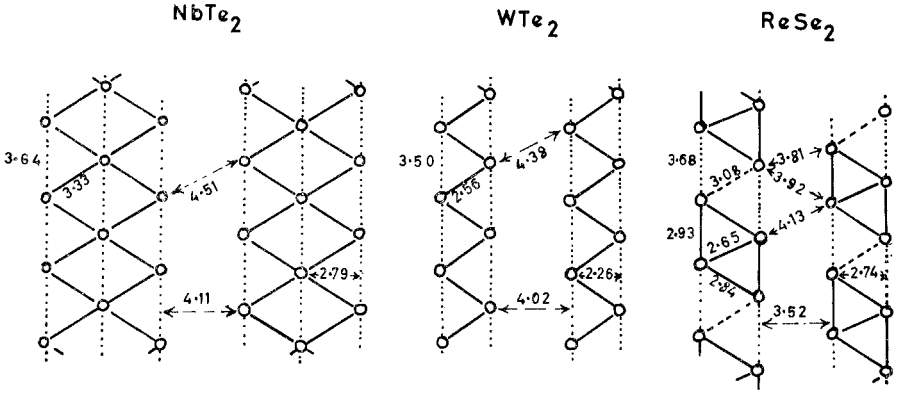

Comparison of the distortion in the metal atom sheets for the layer structures of $NbTe_2$, WTe_2 and $ReSe_2$. (The sheets are actually slightly buckled —see figs. 4, 5 and 6.)

In group VI the 5d compound (WTe_2) again seems more distorted than the 4d counterpart (β-$MoTe_2$) —a fact which the relative definition of their spectra supports (fig. 22 (*f*)). Figure 29 indicates that the overall width of the d band in $MoTe_2$ is *ca.* 1·5 ev, of which about one-third is occupied. In fact the α form of $MoTe_2$, with its unusual trigonal prism coordination and concommittant split-off d_{z^2} band, may be viewed as a special type of distortion semiconductor. This again would emphasize the very unusual position of the trigonal prism metals like $NbSe_2$ (contrast VSe_2 or 1T–$TaSe_2$,

see § 8.2). Actually WTe_2 and β-$MoTe_2$ are not semiconductors but semimetals (cf. MoO_2), with the result that their resistivities have rather low values $\sim 2 \times 10^{-3}\,\Omega$-cm; the room temperature Seebeck coefficients are $\sim 30\,\mu v/°C$. These values are higher than for NbS_2, etc., but very considerably less than for semiconductors like MoS_2. The resistivity plot of

Fig. 73

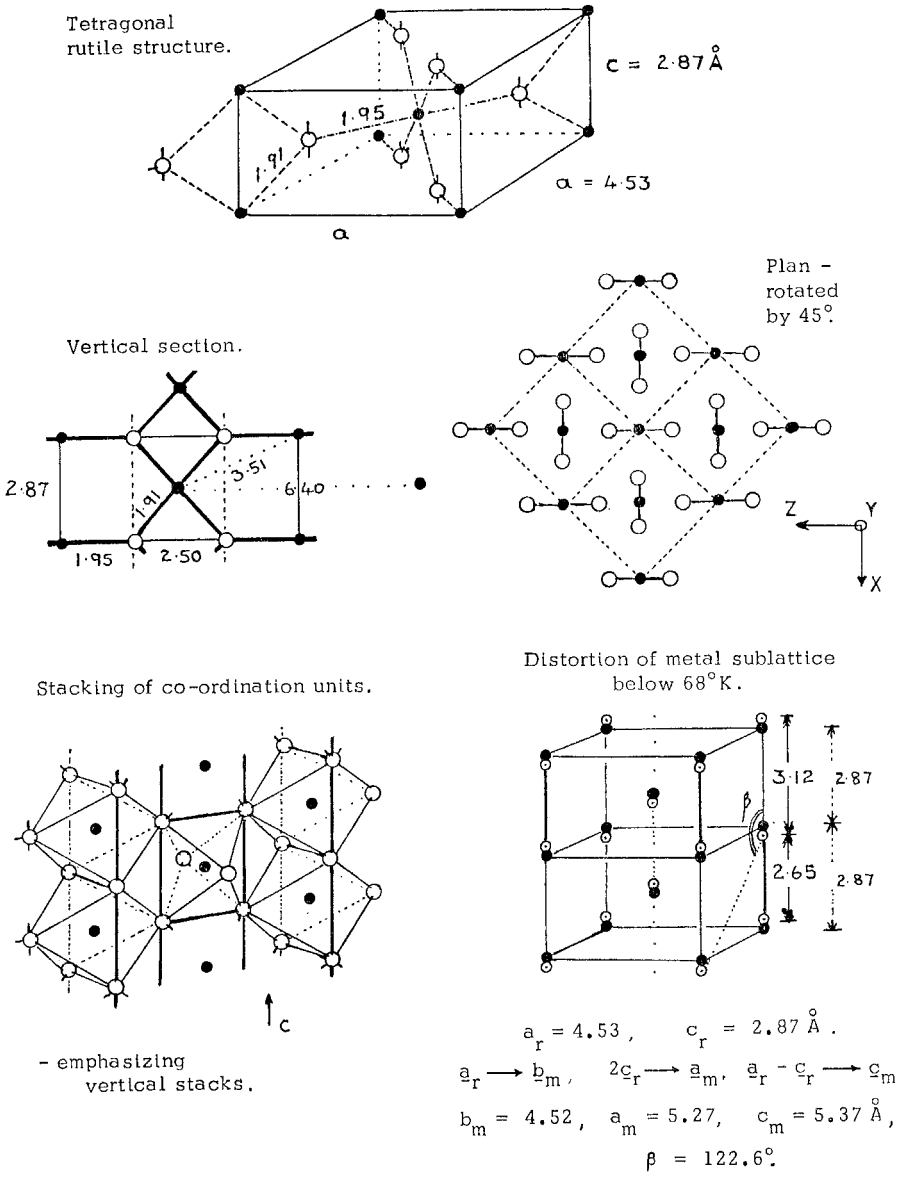

The structure of VO_2 above and below its distortion temperature.

fig. 74 shows the large and rapid change over from the α to the β phase on replacing Mo by W in the mixed system (Mo/W)Te_2. Figure 75 indicates that WSe_2 is considerably more removed from adopting the β form than is $MoTe_2$. From such mixed crystals it has been possible to estimate the position of the A and B excitons in the unknown α form of WTe_2.

No attempts have yet been made to see if any of these distorted layer compounds undergo a reversion within the octahedral β phase to an undistorted condition at very high temperatures. A specimen of (β-) WTe_2

Fig. 74

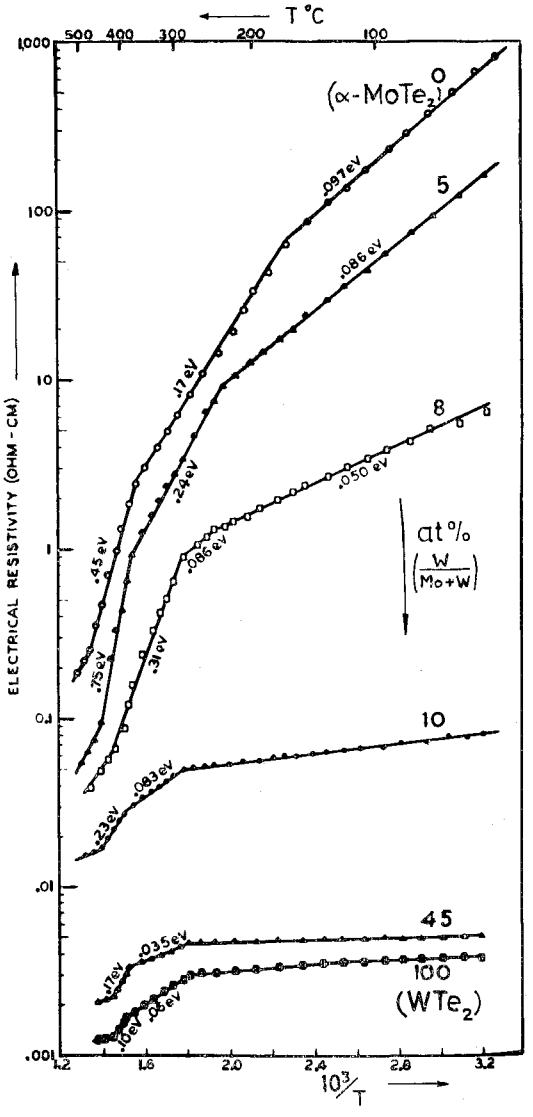

Resistivity in the (Mo/W)Te_2 system. (From Revolinsky and Beerntsen 1964.)

showed no change in its orthorhombic electron diffraction pattern to 800°C. This is not really surprising as the β phase of $MoTe_2$ is only prepared using high temperatures (Revolinsky and Beerntsen 1966) and/or pressures (Silverman 1967).

Fig. 75

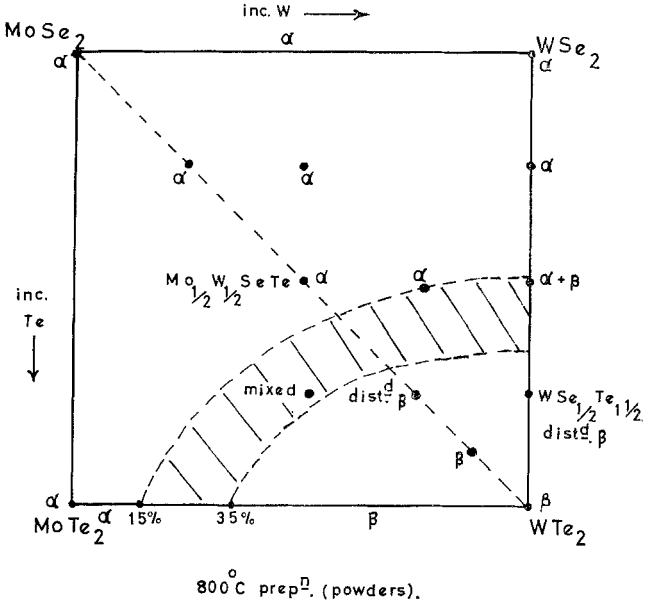

Choice of the α and β structure between $MoSe_2$, WSe_2, $MoTe_2$ and WTe_2. (Based on data of Champion 1965—sintered powders.)

The electrical properties of WTe_2 (Brixner 1962, Kabashima 1966) are very interesting and may be explained, as mentioned earlier, using a semi-metal band model, shown in fig. 76. Above room temperature high thermal excitation from the lower to the upper d sub-bands ($E_a \sim 0{\cdot}1$ ev) causes the material to behave like a highly degenerate semiconductor, with falling resistivity and Seebeck coefficient. The fall in Hall coefficient cannot be simply interpreted due to the mixed carrier situation (cf. p. 269), but Kabashima obtained the fitted curve shown in fig. 76 with the data given below it. The high excess of p type carriers ($\sim 10^{20}/cm^3$) which determines the low temperature properties, corresponds to Brown's metal deficient finding (1966) on the stoichiometry of transport crystals of these compounds.

The group V compounds $NbTe_2$ and $TaTe_2$ again are semi-metals similar to WTe_2, but their conductivity (Brixner 1962) is an order of magnitude higher, being $\sim 10^{-4}\,\Omega$-cm rather than 10^{-3}, as one might expect with an odd electron number†. The conductivity continues falling metal-wise to at

† VTe_2 is also a distorted layer compound though little as yet is known about it (see Røst *et al.* 1964).

least 600°C. Crystals of $NbTe_2$ and $TaTe_2$ are very opaque in the visible part of the spectrum, indicating possibly that free-carrier absorption encroaches into this region. This was not the case for the trigonal prism full metals, like NbS_2, but resembles octahedral VSe_2. WTe_2 was quite highly transparent at 2 μ; presumably a free-carrier absorption edge is to be found in this case at about 5 μ, as is appropriate for a material with $\sim 10^{20}$ carriers per cm^3. Despite its distorted structure $NbTe_2$ is reported to be a superconductor, $T_s = 0{\cdot}74$ °K (van Maaren and Schaeffer 1967). Like WTe_2 and ReS_2, $NbTe_2$ and $TaTe_2$ are diamagnetic (see figs. 61 and 63). VTe_2

Fig. 76

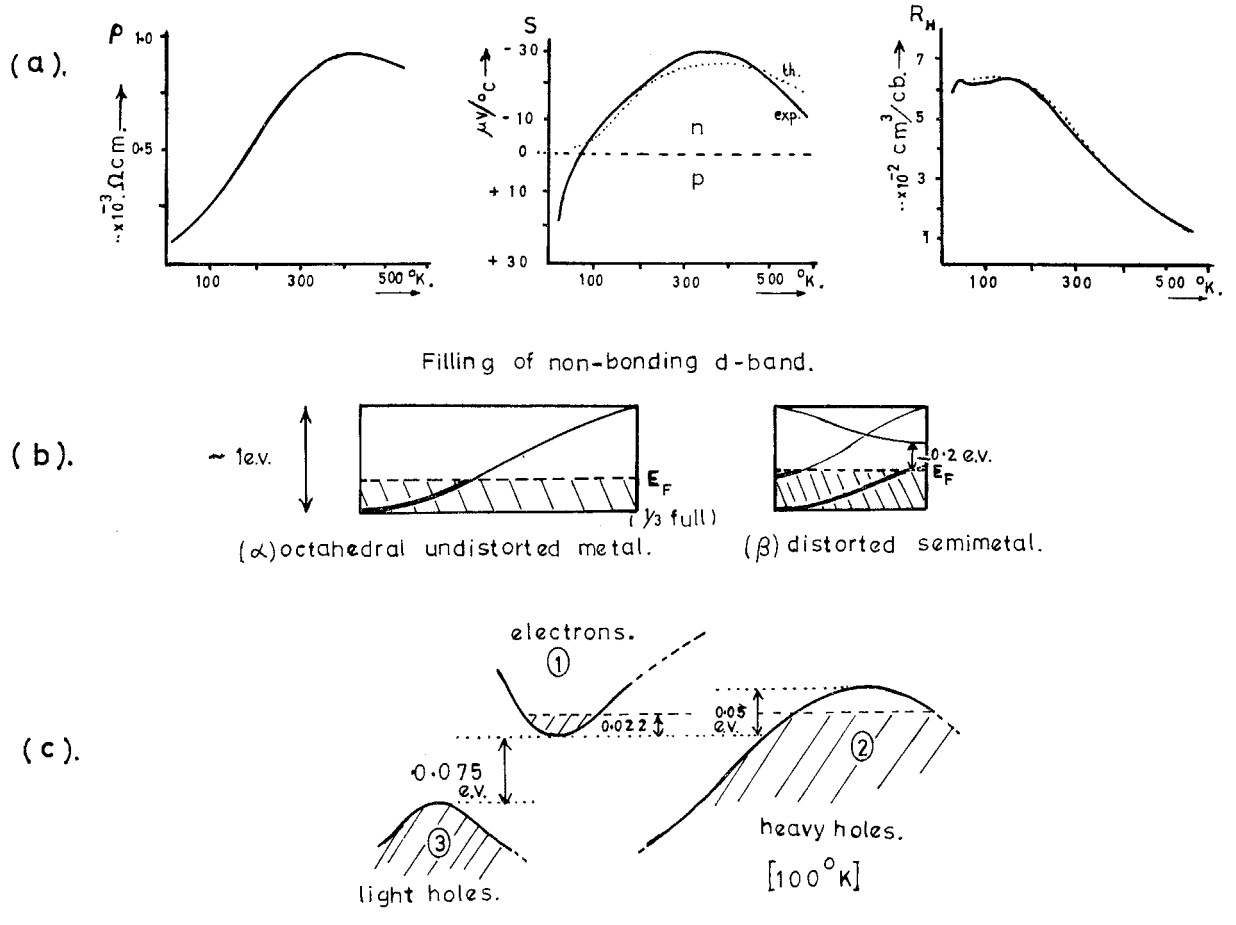

Electrical data and band model for WTe_2. (*a*) ρ, S and R_H versus T (Kabashima 1966), (*b*) possible effect of distortion on the ' non-bonding ' d band of WTe_2, (*c*) model used by Kabashima to fit experimental data. [$\mu_1/\mu_2 = 6$, $\mu_3/\mu_2 = 25$, $m_1 = m_0$, $m_2 = 3m_0$, $m_3 = 0{\cdot}8m_0$.]

Fig. 77

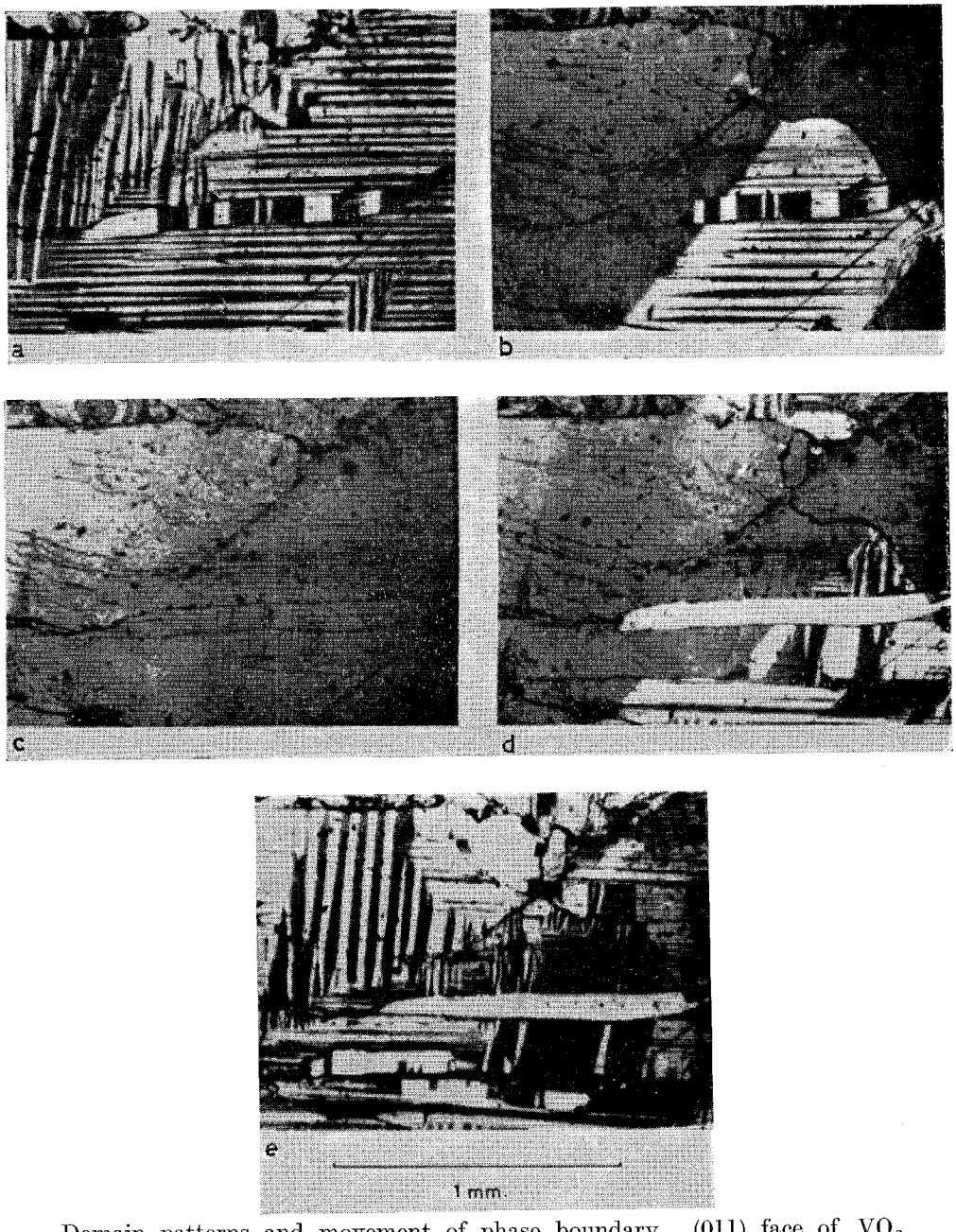

Domain patterns and movement of phase boundary. (011) face of VO_2. (*a*) At room temperature, (*b*) phase boundary moving across sample near 70°C, (*c*) high temperature phase, transition complete, (*d*) during cooling through transition, and (*e*) after cooling, at room temperature. (Viewed by polarized light.)

$NbTe_2$ Fig. 78 (i)

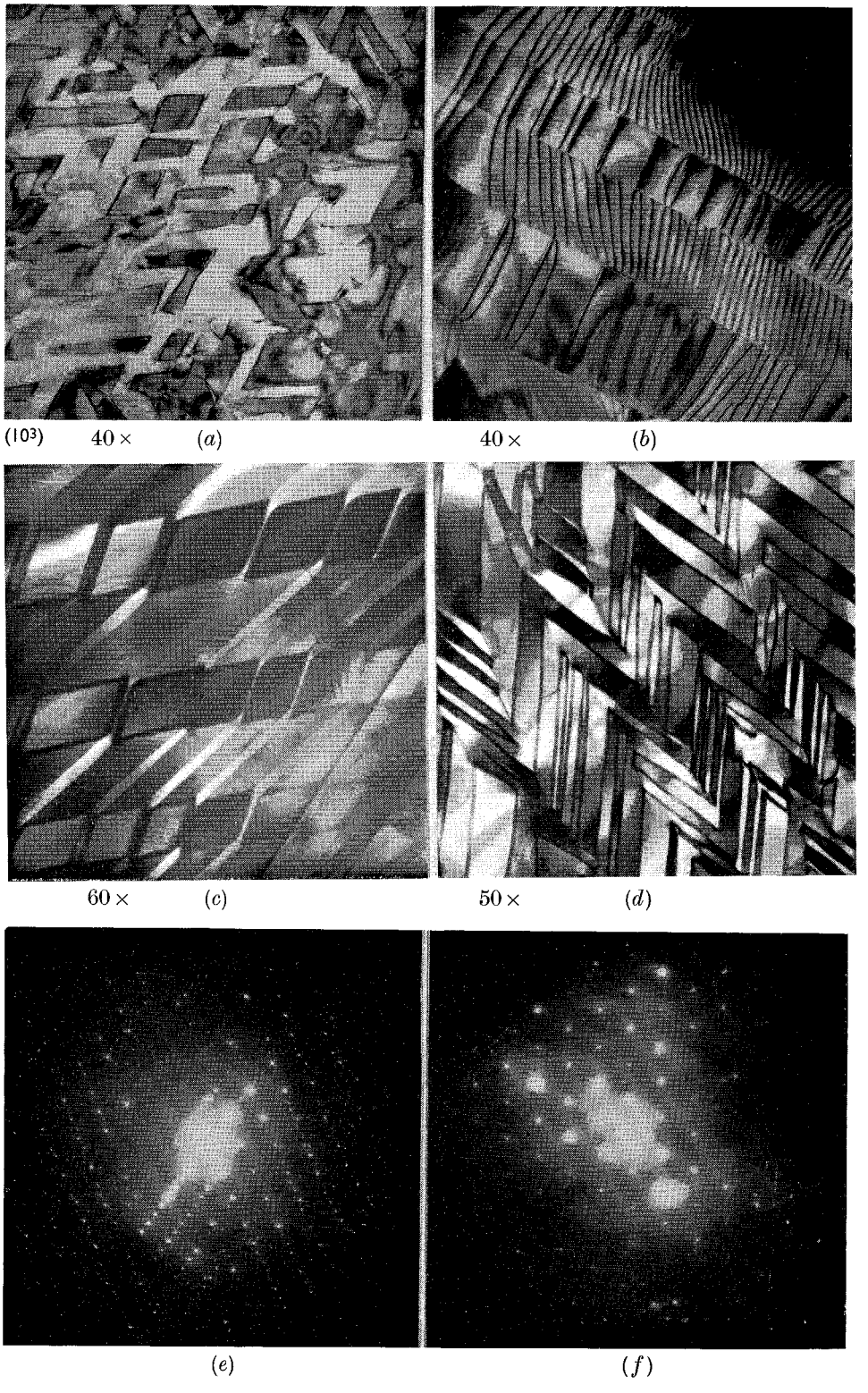

(103) 40× (*a*) 40× (*b*)

60× (*c*) 50× (*d*)

(*e*) (*f*)

Distortion twin 'domains' in $NbTe_2$ and $TaTe_2$. (i) $NbTe_2$. Diffraction pattern (*f*) comes from the region shown in (*d*), but (*e*) is more typical.

$TaTe_2$ Fig. 78 (ii)

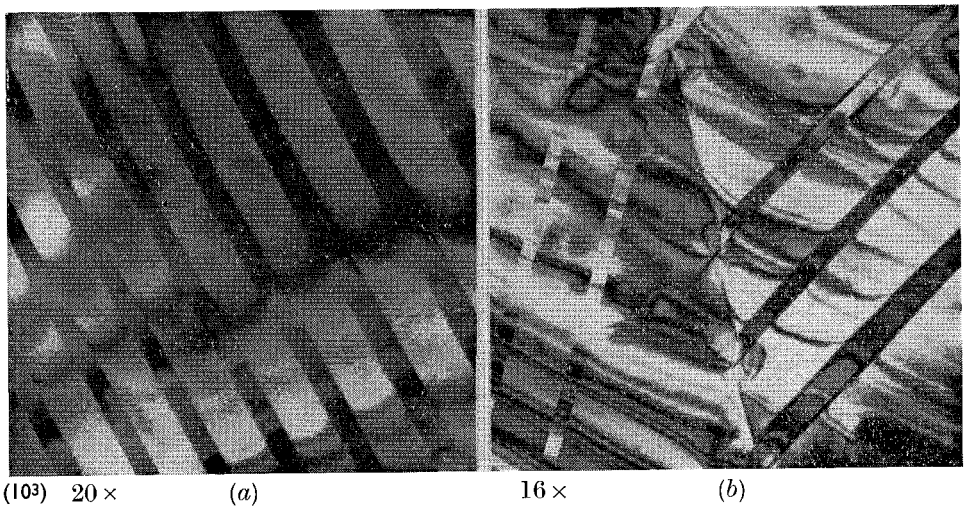

(103) 20× (*a*) 16× (*b*)

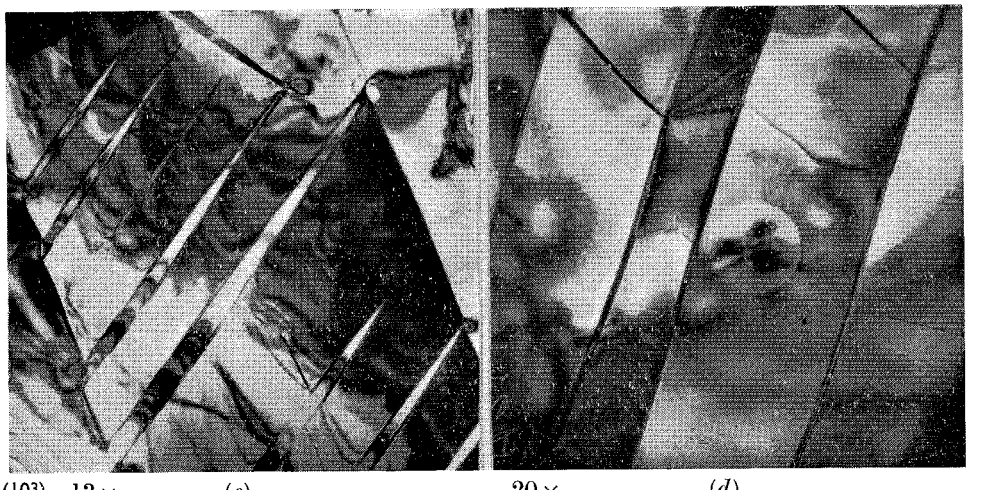

(103) 13× (*c*) 20× (*d*)

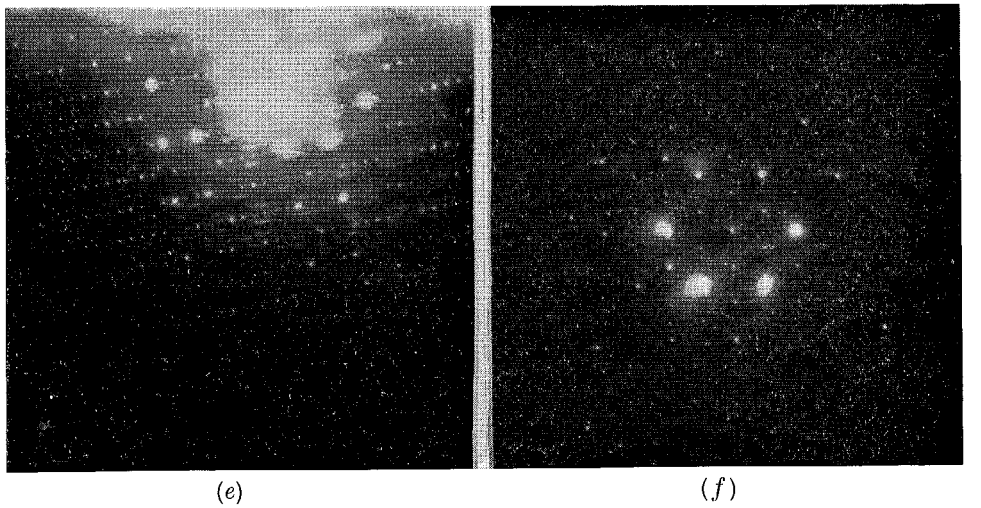

(*e*) (*f*)

(ii) $TaTe_2$. Larger domains than $NbTe_2$. Pattern (*f*) comes from region shown in (*d*) but (*e*) is more typical.

differs in being paramagnetic with a break in χ at 200 °C, somewhat resembling the behaviour in VSe_2 and VO_2, the latter being paramagnetic in both in semi-metallic and distorted semiconducting phases†. Paramagnetism in 3d compounds giving way to diamagnetism in 4d and 5d compounds is not an uncommon feature (see p. 308).

$NbTe_2$, $TaTe_2$ and VO_2 are similar in that they show marked twinned distortion domain formation. Fillingham (1967) has obtained (using reflected polarized light) the fascinating sequence of pictures on VO_2 which are shown as fig. 77. No undistorted domain free phase has been obtained for $NbTe_2$ and $TaTe_2$. Domains have been observed throughout all samples of these layer dichalcogenides and some electron micrographs of these are shown in fig. 78. The domains tend to be smaller in $NbTe_2$ than in $TaTe_2$ and very complex diffraction patterns can result. The absence of domains in our specimens of ReS_2 and WTe_2 may mean that these crystals were grown below the distortion temperature, whereas the $NbTe_2$ and $TaTe_2$ had been quenched from above this temperature. High temperature electron microscopy should resolve this point. Ferromagnetic domain patterns in the insulating layer compound $CrBr_3$ show up very similar to the above (Fischer 1969). As yet antiferromagnetic domains have not been looked for in $NbSe_2$, etc. between the Néel and superconducting transition temperatures.

8.2. *The Properties of 1T–TaS_2 and $TaSe_2$*

We have discussed above cases where distortion of the metal atom sub-lattice leads to the formation of sub-bands from a fairly narrow degenerate d band. A similar removal of free carriers from the system may also be achieved through magnetic coupling and the appearance of antiferromagnetic order. α-NiS is a material of this type, showing a resistivity that rises metal-wise with temperature above the Néel point of 268°K, but rises semiconductor-wise on cooling below this temperature (Sparks and Komoto 1968). There is also a sharp resistivity discontinuity factor of about 50 at T_N. This is unlike the behaviour of $NbSe_2$, etc. which remain metals in the antiferromagnetic phase (see fig. 60 (*b*)). Behaviour like that of NiS may possibly be found in the group IV layer halides α-$TiCl_3/Br_3$ (see § 9.3), but in a group V layer dichalcogenide like $NbSe_2$ (where there is also one non-bonding electron), delocalization just prevails. The word 'just' has been added here because it is known that TaS_2, $TaSe_2$ (and recently $NbSe_2$) may be obtained by quenching from high temperatures in an octahedral modification which promises to show very unusual properties.

Structure analyses (Jellinek 1962, Bjerklund and Kjekshus 1967, Huisman and Jellinek 1969) on these 1T forms have hitherto indicated that they are regular CdI_2 type materials, like VSe_2, and an x-ray powder pattern to this effect is included in fig. 18. However, the spectrum of

† VTe_2 (Røst *et al.* 1964) ; VSe_2 (Røst and Gjertsen 1964) ; VO_2 (Hyland 1968).

Fig. 79

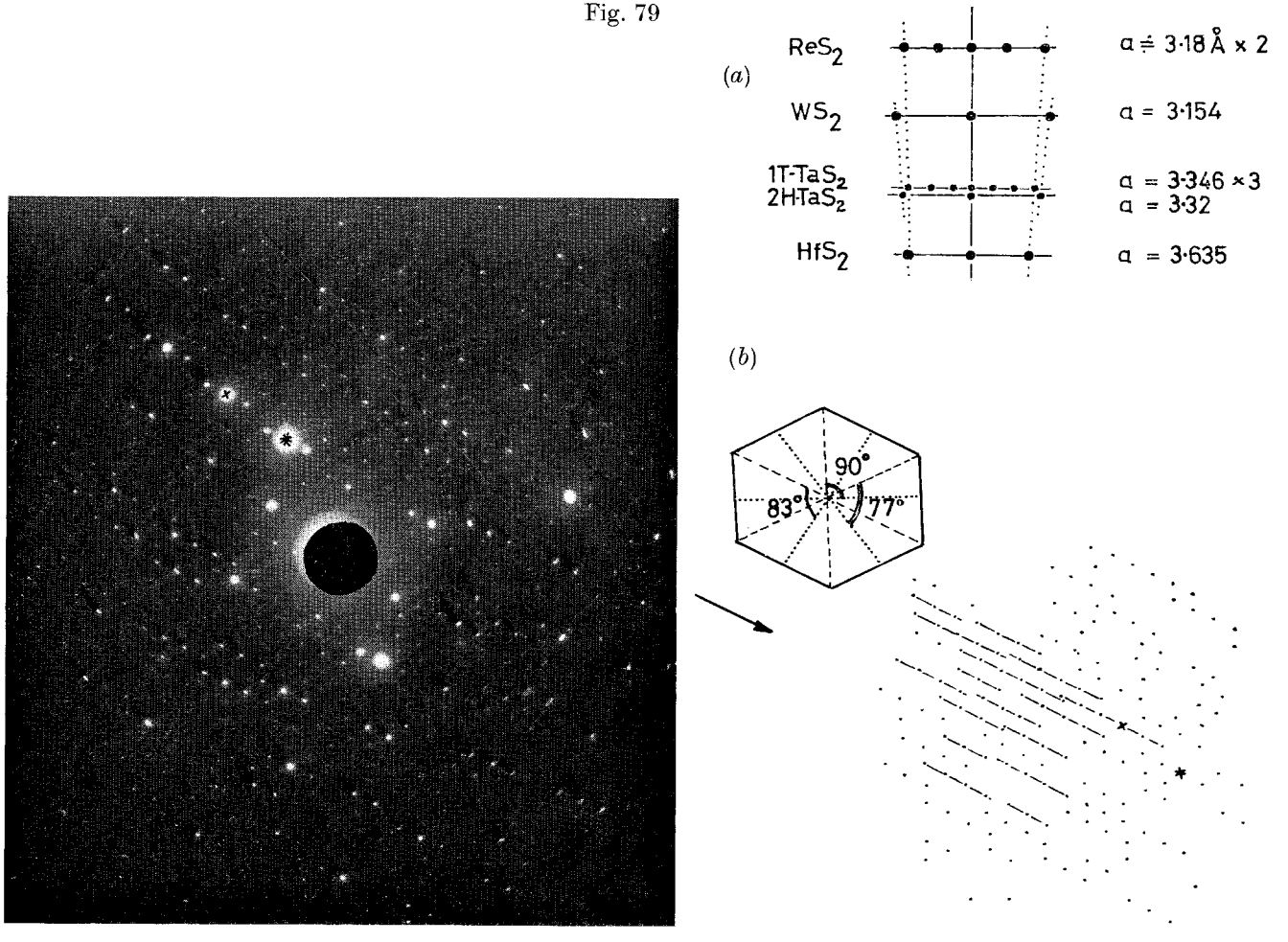

(*a*) Comparison of electron diffraction spot spacing from crystals of HfS_2, TaS_2, WS_2 and ReS_2. (*b*) Electron diffraction spot misalignment in 1T–TaS_2.

1T–TaS_2 given in fig. 22 (*i*) shows that there is no similarity with the metal VSe_2 (or indeed with 2H–TaS_2); the optical absorption of the 1T form is actually falling rapidly in the region of 2 μ. This recalls the behaviour of the semi-metal WTe_2. As yet no infra-red or electrical measurements have been made on these 1T materials, but the resistivity is considerably higher than for the trigonal prism forms†. Further to the above, the 1T form of $TaSe_2$ is known to be diamagnetic (see fig. 63), unlike VSe_2 and 2H–$TaSe_2$ which are Pauli paramagnetic. One possibility to account for the non-metallic properties is that electron–electron correlation in the d band secures at high temperatures (where the mobility is low) a condensation of carriers into electron–hole pairs, i.e. into something like the Mott condition. Certainly for the quenched high temperature 1T phase the metal–metal atom distance is slightly greater than it is in the various trigonal prism polytypes (see table 3). This is compatible with a somewhat smaller band width and greater correlation. However, a simple comparison is not possible; in the 1T case the d band in question is only one-sixth full, in the trigonal prism case it is just half-full. The 1T materials are only metastable at room temperature, and revert to a trigonal prism phase on warming to about 200 °C (see fig. 82). The ease of formation of the 1T phase seems to rise along with the degree of ionic character through the sequence $NbSe_2$, $TaSe_2$, TaS_2. Despite the apparent lack of metallic properties 1T–TaS_2 is reported to be a superconductor below 0·8°K.

Some relief to this impasse comes from an electron microscope investigation of these materials. In spite of the accumulated x-ray data it is clear from the electron diffraction patterns that the structure is not a simple CdI_2 type. The pattern for 1T–TaS_2, included in fig. 19, shows evidence of a hexagonal super-cell with sides perpendicular to *c* of about 10 Å. This super-cell incorporates nine basic cells—see fig. 79. However, whatever process defines the superlattice it must be slight as the simple x-ray pattern fails to detect it. A neutron diffraction result is awaited with interest. One feature which is to be noticed on the electron diffraction patterns is that the strings of spots do not appear to be quite colinear but fall into groups of six or so ending in slight mis-matches. This type of diffraction pattern has been noted for 'shear structures' (cf. 'Nb_2O_5', 'Ta_2O_5)', Spyridelis *et al.* 1968). Goodenough (1967 b) has given a preliminary outline of the reasons for shear structure occurrence in compounds with narrow d bands. Another possibility for the explanation of the properties of 1T–TaS_2 is that it is an example of a so-called 'excitonic insulator' phase. The possibility of such a phase is the subject of a recent review article by Halperin and Rice (1968), but it is as yet without a representative; its feasibility has indeed been queried by Kübler (1969). The basic condition required for the appearance of the phase is that there exists in the material a pair of bands with an energy separation which is less than the binding energy of the

† See for example van Maaren and Harland.

Fig. 80

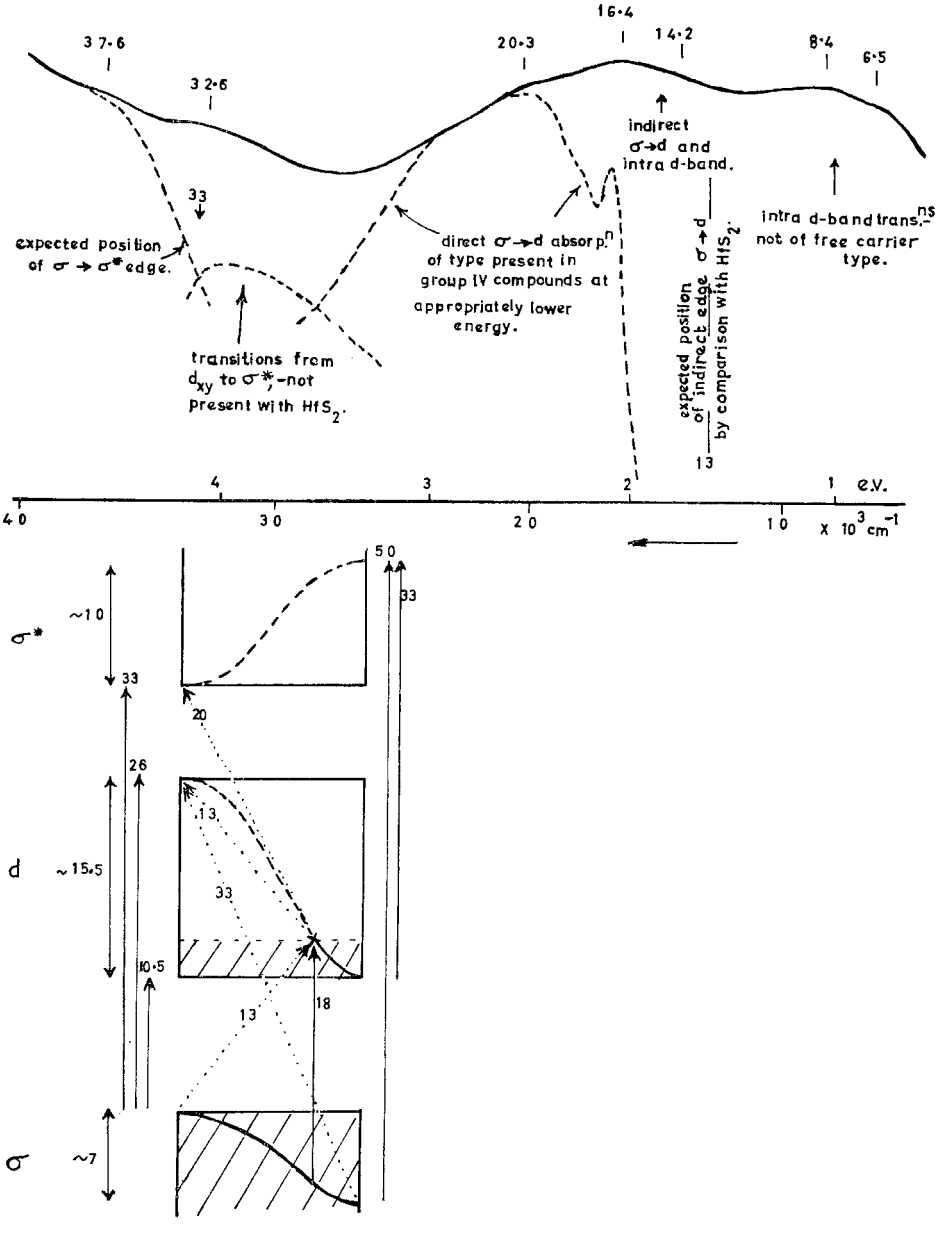

Transmission spectrum of 1T–TaS_2 compared with that of HfS_2.

excitons formed from the band extrema in question†. A new ground state is formed in such conditions with insulating properties, and based on a supercell that has its repeat unit determined by the k separation in the Brillouin zone of the two-band extrema. Clearly the super-cell may thus be incommensurate with the units of the basic cell. Superconductivity in such a system could well arise through Ginzburg's exciton mechanism. The two closely adjacent bands which are required could arise in 1T–TaS_2 following a Mott type condensation of the electron gas, a narrow filled d band separating off from the bulk of empty d states.

Fig. 81

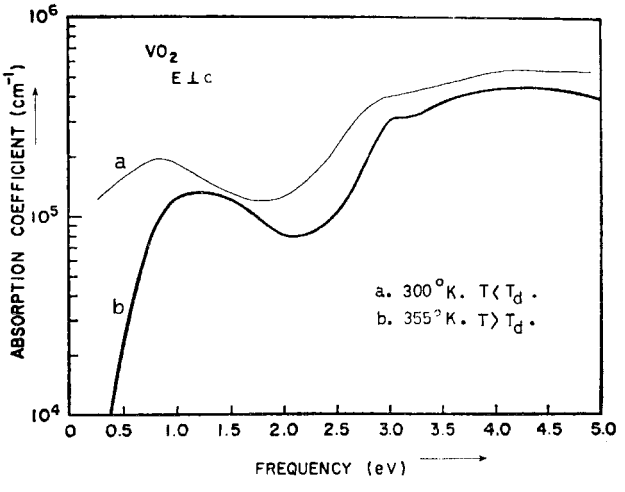

Absorption coefficient of VO_2. (Calculated from reflectivity measurements—Verleur *et al.* 1968.)

As mentioned above, the optical spectrum of 1T–TaS_2 sheds interesting light on this problem. It is seen by reference to fig. 80 that the spectrum above 1·8 ev can be satisfactorily accounted for using the band diagram for HfS_2 (suitably scaled down in energy), now with the d band partially occupied. Absorption occurs then in 1T–TaS_2 around 30 000 cm^{-1} which is absent in HfS_2, involving d to σ^* transitions. The additional absorption found below 13 000 cm^{-1} can only arise *within* the d band system. However, this fairly strong absorption does not appear to be of the normal free-carrier type, as obtained for the trigonal prism metals. In fact absorption falls steeply in 1T–TaS_2 for energies below 1 ev. This was quite unexpected since the 1T carriers should lie in a band that is considerably wider than the trigonal prism d_{z^2} band. In VSe_2, indeed, absorption does remain strong at 2 microns (though the stoichiometry of this compound is somewhat suspect).

† For the possibility of excitonic insulator phases occurring in $MoTe_2$ see p. 251.

This fall in absorption for 1T–TaS_2 is reminiscent of that for the absorption coefficient of VO_2 over this region when in its so-called 'metallic' high temperature state—see fig. 81 (Verleur *et al.* 1968—following an analysis of reflection data). It is becoming clear that this latter compound too is not a simple metal; Hall coefficient measurements indicate a free-carrier density only one-tenth of that expected (see Barker *et al.* 1966, and contrast 2H–$NbSe_2$, p. 272). Optical absorption measurements on 1T–TaS_2/Se_2 are shortly to be carried further into the infra-red.

Another puzzling result has been the optical absorption of the 6R form of $TaSe_2$ (fig. 22 (*i*)). This polytype has alternating trigonal prism and octahedral sandwiches (see fig. 3). However, although the spectrum fits closely to the 2H form above 2·5 ev, below 2·5 ev it resembles that of the 1T form; in particular the free-carrier rise is absent. Huisman and Jellinek (1969) find that the magnetic properties are also intermediate between the 2H (paramag) and 1T (diamag) forms. These workers have carefully investigated the conditions under which the various polytypes occur, and they find that the mixed coordination 4Hb and 6H types are indeed intermediates

Fig. 82

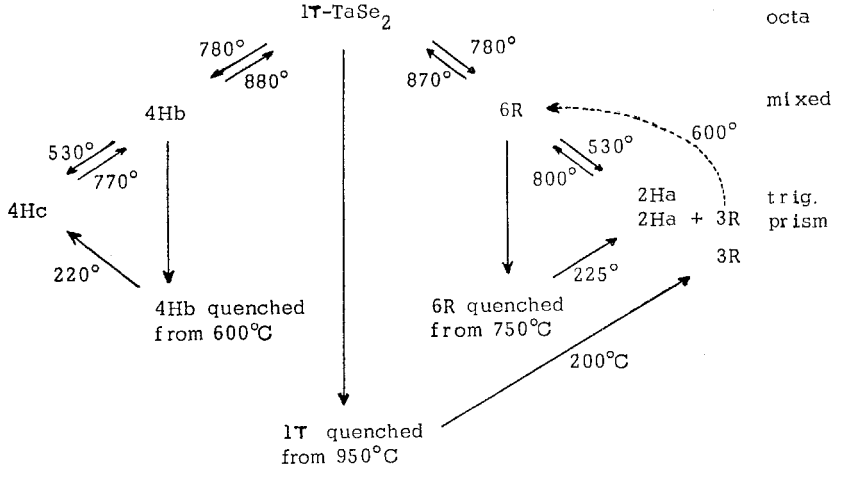

	4Hc	4Hb	1T	6R	2Ha	3R	4Ha
Vol./formula unit.	65·27	65·07	65·66	65·20	64·90	65·31	64·93
a	3·436	3·455	3·477	3·456	3·436	3·435	3·436
c	$4\times6{\cdot}383$	$4\times6{\cdot}287$	6·272	$6\times6{\cdot}304$	$2\times6{\cdot}348$	$3\times6{\cdot}392$	$4\times6{\cdot}350$
c/a	$4\times1{\cdot}858$	$4\times1{\cdot}820$	1·804	$6\times1{\cdot}824$	$2\times1{\cdot}847$	$3\times1{\cdot}861$	1·848

4Hc and 2Ha are stable room temperature forms.

Polytypic transformations in the $TaSe_2$ system. (Based on data by Huisman and Jellinek 1969.)

between the 1T and the 4Hc and 2Ha forms (fig. 82). 3R appears to be metastable at all temperatures. The irreversible 1T→3R transition makes itself apparent in fig. 63. One interesting finding is that given samples are reversible in one or other of the two channels 4Hb↔1T, and 6R↔1T. This 'memory' return from the 1T form could possibly arise from slight stoichiometric differences or from the stacking defect patterns. Clearly a detailed single crystal structure analysis of 1T–TaS_2 at high and low temperatures is called for on all counts. The possible effects of high pressures on polytype stability are also not clear. From the lattice parameters alone, it would seem that uniaxial pressure $\|c$ favours octahedral coordination, whereas isotropic pressure would favour trigonal prism coordination.

We also hope to gain further insight into the octahedral state by studying the mixed IV–V system (Ta/Ti)S_2. It is possible that the unusual properties of 1T–TaS_2 only arise when there is exactly the integral electron number per metal atom (cf. NiS_2, § 9.1).

§ 9. Cause and Effect of Crystal Structure Choice among the Transition Metal Dichalcogenides and Halides

9.1. *Survey of the Properties of the Transition Metal Dichalcogenides beyond Group VII*

It is in this part of the family that the non-layered structures are found. Actually the manganese compounds of group VII take the pyrites structure, but they form a special case unique to the whole family, in that they possess a high degree of ionicity, based on the very stable $Mn^{2+}d^5$ half-shell. All three manganese compounds are insulators, despite the odd electron number, so reflecting the localized character of the d electrons. This is also supported by their magnetic properties. They show the full paramagnetism of the d^5 ion, and only become antiferromagnetic on the low side of 100°K (Hastings *et al.* 1959, Lin and Harker 1968). It is not known whether they give salt-like ligand field spectra as exhibited by MnO (Iskenderov *et al.* 1968) and $\alpha/\beta/\gamma$ MnS (Ford *et al.* 1963)—compounds which again are much more ionic than their immediate neighbours in the Periodic Table. MnS_2 is in fact deep red. Two is not a stable valency for the heavier elements of group VII, Tc and Re, and as was seen in § 8 the dichalcogenides of these elements are completely different from those of Mn.

$MnTe_2$ is the least ionic of the manganese compounds, and has a room temperature resistivity of only *ca.* 1 Ω-cm (always p type—Johnston *et al.* 1965). Under pressure the conductivity rises, and the Néel temperature quickly shifts to temperatures above 100°K (Sawaoka *et al.* 1966). Indeed the break in the latter plot at 100 kB may mark the onset of collective band behaviour in $MnTe_2$.

The remaining compounds in question are set out in table 15. There the crystal structures are given, and heavy type has been used to indicate the semiconductors. The first part of the table, (*a*), arranges these materials

Table 15. Structures of the group VIII transition metal dichalcogenides classified by (*a*) group number, (*b*) period number

(*a*)

VIII a d^6	FeS_2 **M, P** RuS_2 **P** OsS_2 **P**	$FeSe_2$ **M, (P–H.P.)** $RuSe_2$ **P** $OsSe_2$ **P**	$FeTe_2$ **M, (P–H.P.)** $RuTe_2$ **P** $OsTe_2$ **P**
VIII b d^7	CoS_2 P (RhS_2) P IrS_2 **X**, (P–H.P.)	$CoSe_2$ P, M $RhSe_2$ **X**, (P–H.T.) $IrSe_2$ **X**	$CoTe_2$ M, (C–H.T.), (P–H.P.) $RhTe_2$ P, (C–H.T.) $IrTe_2$ C
VIII c d^8	NiS_2 **P** PdS_2 **Y**, (Y′–H.P.) PtS_2 **C**	$NiSe_2$ P $PdSe_2$ **Y** $PtSe_2$ **C**	$NiTe_2$ C, (P–H.P.) $PdTe_2$ C $PtTe_2$ C
I d^9	CuS_2 (P–H.P.)	$CuSe_2$ M, (P–H.P.)	$CuTe_2$ (P, C–H.P.)
II d^{10}	ZnS_2 **(P–H.P.)** CdS_2 **(P–H.P.)**	$ZnSe_2$ **(P–H.P.)** $CdSe_2$ **(P–H.P.)**	$ZnTe_2$ **(P–H.P.)** **(C–H.P.)**

Structures: P: pyrite, M: marcasite, X: $IrSe_2$, Y: PdS_2, C: cadmium iodide. Unusual preparation conditions: H.T.: high temperature >900°C, H.P.: high pressures ~50 kB, often coupled with high temperatures. Semiconductors are printed in heavy type.

(*b*)

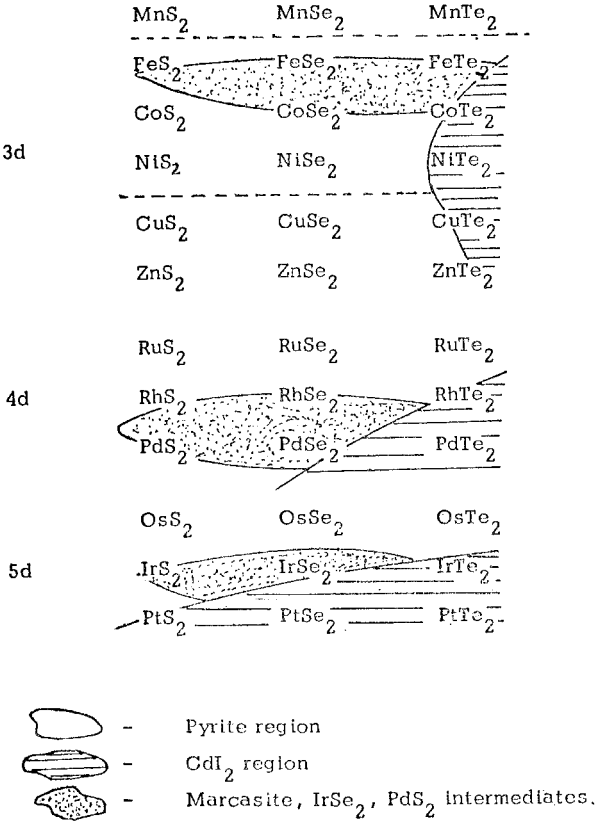

by group number, and the second part, (*b*), indicates the development of structure type over the periods 3, 4 and 5. As mentioned earlier (see figs. 7 to 11), the marcasite, $IrSe_2$ and PdS_2 structures are intermediate between those of cadmium iodide and pyrites. The prominence of the pyrite structure among the 3d materials is lost in the 'heavier' periods.

A considerable amount of fairly detailed work has appeared recently on the 3d materials, particularly in the pyrite phase†, but there is little published as yet on several of the heavier compounds. The pyrite structure is not one confined to transition metal elements (e.g. SiP_2, Donohue *et al.* 1968), but represents a general geometrical 'attempt' at high density 6 : 4 packing. As seen from the above example the structure requires 14 valence electrons, 12 being equivalent to the M–X bonding of the octahedra, and two to the X–X link (see fig. 7). FeS_2 with 20 electrons, then has six surplus electrons which enter the d bands inserted within the basic $\sigma\sigma^*$ gap. This gap is likely to be about 3–4 ev wide. The t_{2g} orbitals form a true non-bonding band, but the upper band based on the e_g orbitals will take on a slight anti-bonding character due to the covalent participation in the M–X

Fig. 83

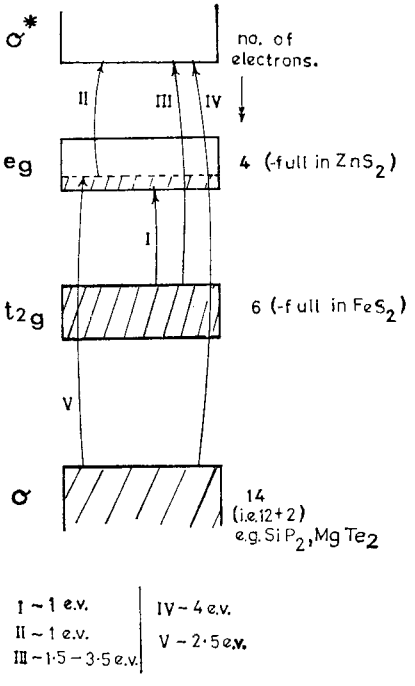

Postulated banding for the pyrite disulphides. (Based on optical and electrical data from Bither *et al.* 1968.)

† See Miyahara and Teranishi (1968) ; Jarrett *et al.* (1968) ; Bither *et al.* (1968) ; Adachi *et al.* (1969).

Fig. 84

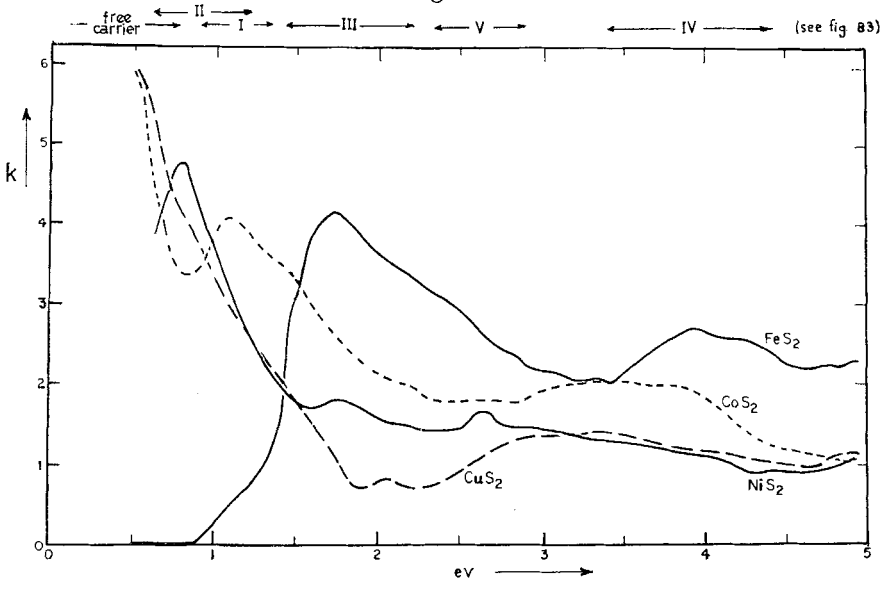

Reflection spectra (reduced to k value) of the 3d pyrite sulphides FeS_2, CoS_2, NiS_2 and CuS_2. (From Bither *et al.* 1968.)

Fig. 85

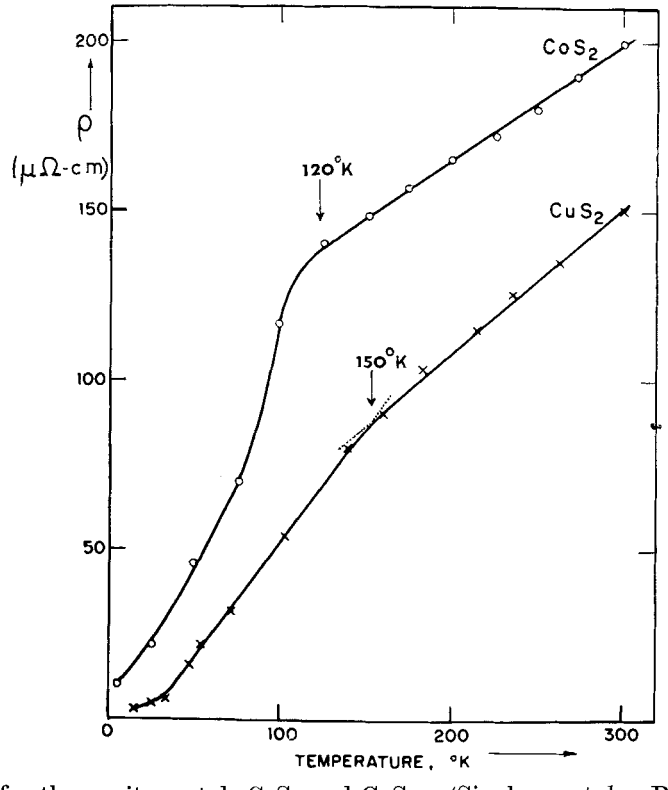

ρ–T plot for the pyrite metals CoS_2 and CuS_2. (Single crystals—Bither *et al.* 1968.)

bonding, the e_g orbitals being suitably oriented. Thus in the FeS_2 group (VIIIa) we arrive at a semiconducting condition with the t_{2g} band completely filled. Depending on impurity content the specimens can either be n or p type. Electron mobilities are $\sim 200\,cm^2/v\text{-}sec$, with hole mobilities substantially smaller. From optical (fig. 84) and electrical data (see, for example, Bither *et al.* 1968) the inter d band gap is seen to be just under 1 ev wide. FeS_2, then, is in many ways reminiscent of MoS_2. This is even more true of say $RuTe_2$ by which stage the band gap has closed to 0·25 ev (Hulliger 1963, Johnston *et al.* 1965). The band properties of these semiconductors are clearly quite different from the properties of the manganese compounds. The very large lattice parameters of the manganese dichalcogenides (see fig. 12) contrast their high ionicity. Also they share the rather high compressibility of other Mn^{2+} compounds (see Clenenden and Drickamer

Fig. 86

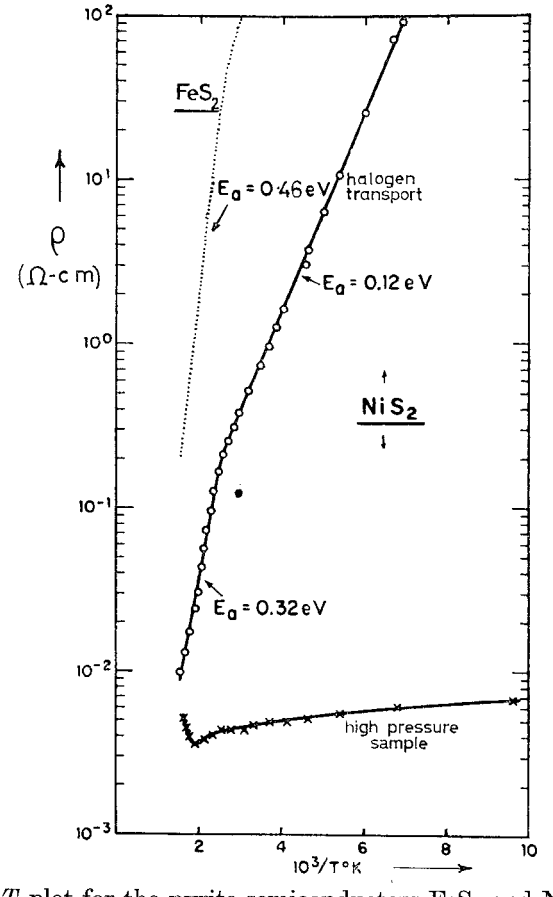

ρ–T plot for the pyrite semiconductors FeS_2 and NiS_2. (Single crystals—Bither *et al.* 1968.)

1966)—compared with which FeS_2 is much more rigid (linear compressibility $2{\cdot}3 \times 10^{-7}$/bar—(Sato *et al.* 1969)†.

Those pyrites with more electrons than FeS_2 take these up into the e_g band (fig. 83). Since this has some anti-bonding character their formation becomes progressively more difficult. Thus the pyrite tellurides of Fe, Co, and Ni, and all the Cu and Zn compounds require high pressures for their formation (Bither *et al.* 1968). The e_g band is full at Zn (d^{10}), and the zinc compounds are diamagnetic insulators (ZnS_2, $E_g \sim 2{\cdot}5$ ev, $\rho \sim 10^6$ Ω-cm). For Co (d^7) and Cu (d^9) the band is one-quarter and three-quarters full respectively, and accordingly metals result. The properties of these metals will be compared shortly with those of group V like NbS_2. The nickel compounds (d^8) in the half-filled band position seem to have very interesting potentialities with regard to the metal–insulator transition. The reflection spectra of these pyrites are shown in fig. 84, and the various features are interpreted there in terms of the banding arrangement of fig. 83.

Fig. 87

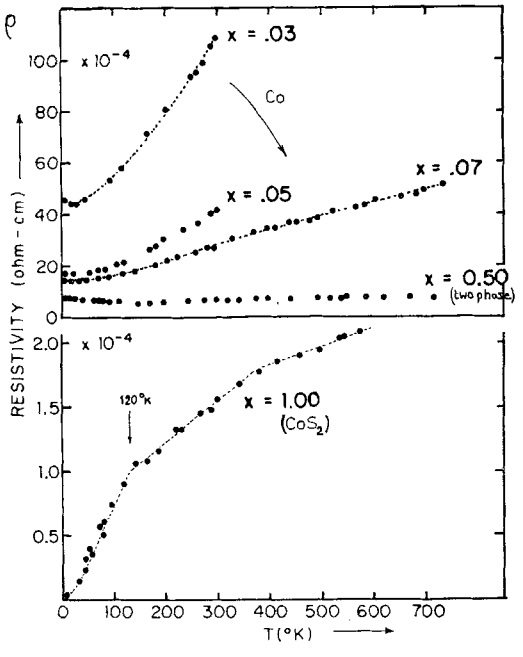

ρ–T plots for FeS_2 doped with Co. (Single crystals—Bither *et al.* 1968.)

† N.B. The low temperature-independent paramagnetism ($\chi_M \sim 10 \times 10^{-6}$ cgs/mole—Miyahara and Teranishi 1968) of FeS_2 is to be found in other narrow band 3d *semiconductors* (e.g. $FeAs_2$[a], TiO_2[b]) and is absent from their broader band diamagnetic 4d and 5d counterparts. (Ref. 'a', Holseth and Kjekshus 1968; Ref. 'b', Senftle and Thorpe 1968.)

It would seem from the occurrence of delocalized and metallic properties in the e_g* band that a fairly high degree of orbital overlap is achieved via the bonded X_2 units. The metal-metal distance along the pyrite cube axes is from 5·5 to 6·5 Å, but this is bisected by the centres of the X_2 pairs (see fig. 7). Even in the t_{2g} non-bonding band metal orbital overlap is presumably still mediated by some non-metal mixing, since the direct metal–metal distances (diagonally across the cell faces) are from 3·8 to 4·7 Å. Figure 13 shows that this is very much greater than the direct metal–metal distance in most of the TX_2 layer dichalcogenides (3·1 to 4·0 Å).

The properties of the disulphide and diselenide 3d pyrites are summarized in table 16, and various features are amplified through figs. 85 to 90. First, it is worth comparing the *metals* CoS_2, CuS_2 and $NiSe_2$, to NbS_2, etc., and also to the rutile metals VO_2, CrO_2, RuO_2. Optical, electrical and magnetic data have been collected into table 17. From this data, augmented by that on certain related compounds, the following list has been drawn up in order of decreasing metallicity from left to right.

$$\underset{\text{good metals}}{ScSe,\ ReO_3,\ RuO_2,\ \overset{\alpha}{\underset{\beta}{RhTe_2}},\ CuS_2,\ \alpha RhSe_2,\ PdTe_2/Te,\ TiO,\ 1T\text{–}TaS_2,}\ \underset{\text{superconductors}}{\rightarrow}$$

$$\ldots\ NbTe_2,\ MoO_2,\ VO_2\ \ CoSe_2,\ CrO_2,\ CoS_2,\ NiTe\ \ldots\rightarrow$$

$$\text{band magnetic}$$

$$\ldots\ ?\ NiSe_2,\ NiS\ \ NiS_2,\ \alpha\text{–}TiBr_3,\ NiI_2$$

$$\text{possibly metals under pressure}$$

The positioning of the occurrence of superconductivity and band magnetism here is in line with semi-theoretical conclusions concerning overlap (Goodenough 1966, 1967 a, b, c, 1968 a, b, and nicely demonstrated with the perovskite-type compounds). The difference between the 4d superconductor α-$RhSe_2$ (T_s 6°K) and its 3d magnetic counterpart $CoSe_2$ (T_N 90°K) illustrates well the effect of increased overlap. The very unusual behaviour of $NbSe_2$ is again apparent in showing both superconductivity and antiferromagnetism (see § 7.3)†, though a small moment has been reported by Munson *et al.* (1967) for CuS_2, and Bither *et al.* (1968) also find a break in the ρ–T curve for CuS_2 at 150°K (cf. fig. 85).

† Such behaviour is not entirely unknown, La/Gd alloys showing some coexistence of magnetic and superconducting conditions (cf. Rado and Suhl, Vol. 2B, p. 209; Bennemann *et al.* 1969).

Fig. 88

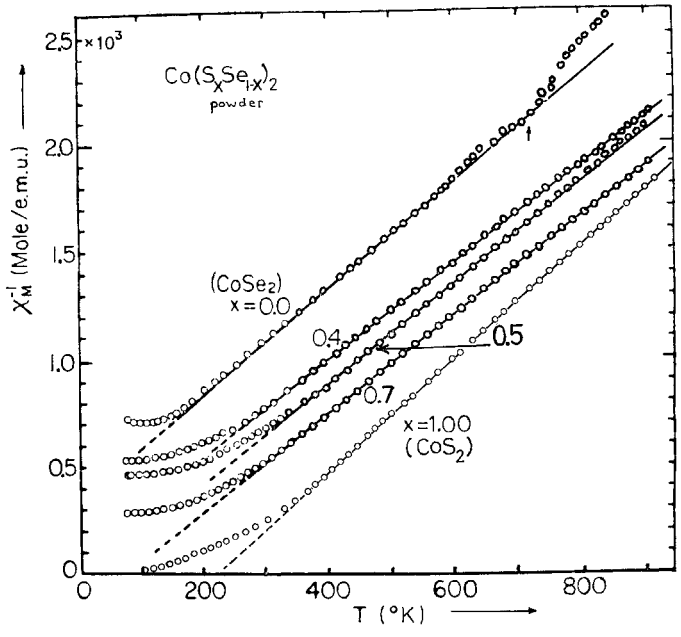

$1/\chi$–T plot for CoS_2, $CoSe_2$ and mixed crystals. (Adachi *et al.* 1969.)

Fig. 89

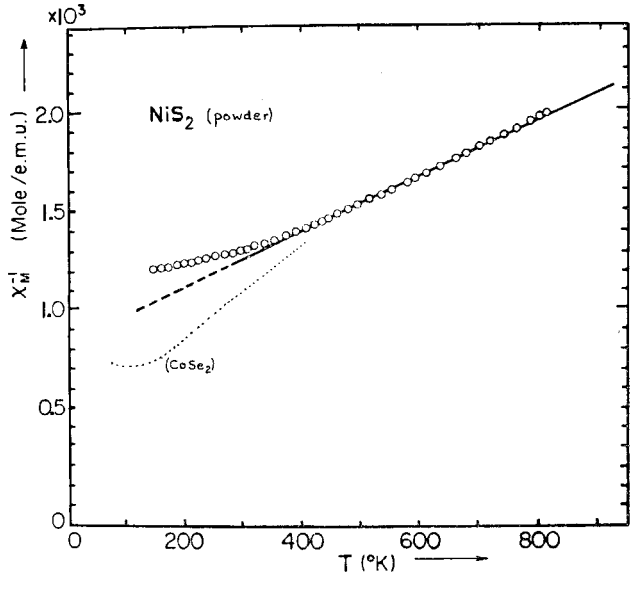

$1/\chi$–T plot for NiS_2. (Adachi *et al.* 1969.)

Mixed crystals such as $(Fe/Co)S_2$, $(Co/Ni)S_2$, $(Ni/Cu)S_2$, $(Cu/Zn)S_2$ have been prepared (Bouchard 1968) and show very interesting gradations of property. As for say MoS_2 with Nb doping (§ 7.3.3), additions of small amounts of Co to FeS_2 rapidly reduce the resistivity, and metallic type

Fig. 90

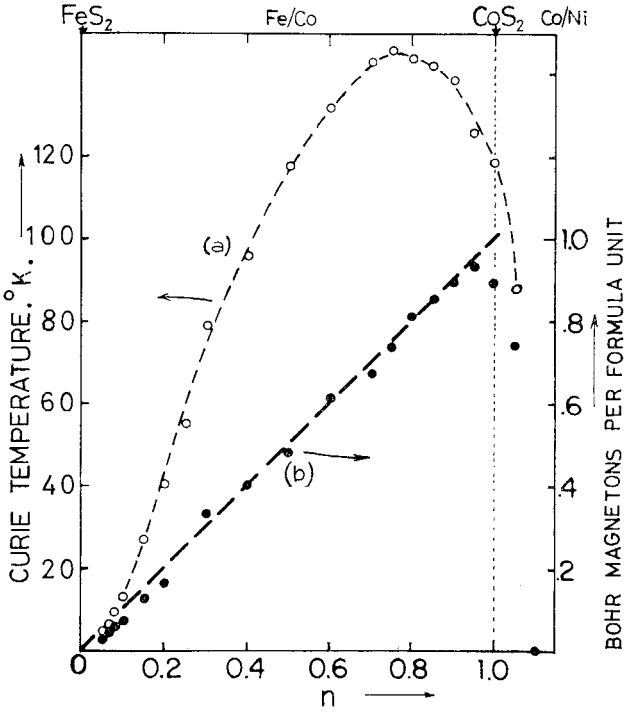

Ferromagnetism in the $(Fe/Co)S_2$ and $(Co/Ni)S_2$ systems. (*a*) Curie temperature versus electron number, (*b*) saturation moment versus n. (From Bither *et al.* 1968.)

temperature coefficients are produced (see fig. 87). Ferromagnetism appears with about 5% Co added, and the magnetic saturation moment, μ_s, corresponds closely to one 'active' electron per added cobalt atom over the composition range 10 to 95%. Beyond this limit μ_s begins to fall rapidly. If we now consider the CoS_2/Ni system this value moves to zero for the addition of only 10% Ni (see fig. 90). The ferromagnetism of CoS_2 is the subject of a recent series of papers (Adachi *et al.* 1969). The Curie temperature T_c falls quite quickly under pressure and particularly so following the replacement of sulphur by selenium (limit of 12% Se). CoS_2 follows the $T^{3/2}$ law for saturation magnetization quite well up to 40°K, leading to an exchange interaction value of $0{\cdot}3 \times 10^{-2}$ev per cobalt pair ($J_{s.w.}$—see Kittel 1967, p. 468). $CoSe_2$ is antiferromagnetic, and as fig. 88 shows, T_N is about 90°K with $\theta_p \sim -160$°K. From fig. 89, NiS_2 would also appear

Table 16. Summary of the properties of the pyrite sulphides and selenides of Fe, Co, Ni and Cu

	Electrical	Magnetic
FeS_2	Semiconductor, $E_g \sim 0{\cdot}9$ ev $\rho^{300\,°K} = 1\ \Omega$-cm $S = 500\ \mu v/°c$	Van Vleck temperature independent paramagnetism, $\chi \sim 10 \times 10^{-6}$ c.g.s. units/mole (Miyahara and Teranishi 1968)
CoS_2	Metal, $\rho^{300\,°K} = 2 \times 10^{-4}\ \Omega$-cm $S = -30\ \mu v/°c$	Ferromagnetic, $T_c = 124°K$ (118°) $\mu_s = 0{\cdot}84\mu_B$ (0·89) $\theta_p = +220°K$ (193°) $p_{eff} = 1{\cdot}76\mu_B$ (1·84) $\frac{\Theta_p}{T_c} = 1{\cdot}64$ (1·77) $\chi^{300\,°K} = 4000 \times 10^{-6}$ c.g.s. units/mole
NiS_2	Semiconductor, (*a*) Sulphur deficient : $E_a > ^{400\,°K} = 0{\cdot}32$ ev $E_a < ^{400\,°K} = 0{\cdot}12$ ev $\rho^{300\,°K} \sim 0{\cdot}5\ \Omega$-cm $S = +300\ \mu v/°c$ (*b*) Sulphur rich : $E_a \sim 0{\cdot}01$ ev $\rho^{300\,°K} \sim 5 \times 10^{-3}\ \Omega$-cm $S = +9\ \mu v/°c$	Paramagnetic, $\theta_p = -740°K$ (1800°) $p_{eff} = 2{\cdot}48\mu_B$ (3·65) $\chi^{300\,°K} = 700 \times 10^{-6}$ c.g.s. units/mole
CuS_2	Metal, $\rho^{300\,°K} = 1{\cdot}5 \times 10^{-4}\ \Omega$-cm $S = +3\ \mu v/°c$ superconductor $T_s = 1{\cdot}5°K$	Pauli paramagnetic, $\chi^{300\,°K} \sim 40 \times 10^{-6}$ c.g.s. units/mole
$FeSe_2$	Semiconductor, $\rho^{300\,°K} \sim 0{\cdot}1\ \Omega$-cm	' Non-magnetic '
$CoSe_2$	Metal, $\rho^{300\,°K} = 1 \times 10^{-4}\ \Omega$-cm $S = -20\ \mu v/°c$	Antiferromagnetic, $T_N = 90°K$ $\theta_p = -160°K$ ($-450°K$) $p_{eff} = 1{\cdot}72\mu_B$ (2·44) $\chi^{300\,°K} = 900 \times 10^{-6}$ c.g.s. units/mole
$NiSe_2$	Metal, $\rho^{77\,°K} = 0{\cdot}7 \times 10^{-4}\ \Omega$-cm $\rho^{300\,°K} = 2{\cdot}2 \times 10^{-4}\ \Omega$-cm $S = -7\ \mu v/°c$	Pauli paramagnetic, $\chi^{300\,°K} = 170 \times 10^{-6}$ c.g.s. units/mole
$CuSe_2$	Metal, $\rho^{300\,°K} = 0{\cdot}8 \times 10^{-4}\ \Omega$-cm $S = +2\ \mu v/°c$ superconductor $T_s = 2{\cdot}4°K$	Pauli paraagnetic, $\chi^{300\,°K} \sim 90 \times 10^{-6}$ c.g.s. units/mole

Based on papers of Bither *et al.* (1968) and Adachi *et al.* (1969). Magnetic data from first paper appear bracketed for CoS_2, NiS_2 and $CoSe_2$.

to be antiferromagnetic, but although χ stops rising below 200°K no sharply defined ordering temperature has been found, and indeed no order is observed by neutron diffraction, even at 4°K (Adachi *et al.* 1969).† As mentioned above the semiconducting properties of NiS_2 are unusual and contrast strongly with the metallic properties of $NiSe_2$ (see table 17). The semiconductivity disappears at the intermediate composition $Ni(S_{0.8}Se_{0.2})_2$ (Hulliger 1965). In the mixed sulphides studied by Bouchard (1968), the

† J. Hastings is about to publish a paper contradicting this finding.

Table 17. Properties of various metallic d band dichalcogenides and oxides

	CoS_2	$CoSe_2$	CuS_2	$NiSe_2$	$NbSe_2$	VO_2	CrO_2	RuO_2	ReO_3
n	1	1	3	2	1	1	2	3	1
$\rho^{4°K}$ (Ω-cm)	$0{\cdot}08\times10^{-4}$		$0{\cdot}05\times10^{-4}$		$0{\cdot}1\times10^{-4}$		$0{\cdot}03\times10^{-4}$	$<0{\cdot}2\times10^{-6}$	
$\rho^{77°K}$ (Ω-cm)	$0{\cdot}7\times10^{-4}$		$0{\cdot}3\times10^{-4}$	$0{\cdot}7\times10^{-4}$	$0{\cdot}4\times10^{-4}$		$0{\cdot}08\times10^{-4}$	$0{\cdot}03\times10^{-4}$	$0{\cdot}3\times10^{-6}$
$\rho^{300°K}$ (Ω-cm)	$1{\cdot}6\times10^{-4}$	1×10^{-4}	$1{\cdot}5\times10^{-4}$	$2{\cdot}2\times10^{-4}$	$1{\cdot}6\times10^{-4}$	[10^2]	$2{\cdot}5\times10^{-4}$	$0{\cdot}4\times10^{-4}$	8×10^{-6}
$\rho^{400°K}$ (Ω-cm)	$1{\cdot}8\times10^{-4}$					1×10^{-4}	10×10^{-4}		
$\alpha\ °K^{-1}$ (300°K)	$1{\cdot}7\times10^{-3}$		$2{\cdot}8\times10^{-3}$	$\sim4\times10^{-3}$	$2{\cdot}8\times10^{-3}$		$9{\cdot}4\times10^{-3}$		
R_H cm³/Cb	$-1{\cdot}1\times10^{-3}$		$-1{\cdot}9\times10^{-3}$		$4{\cdot}5\times10^{-4}$				
	$\equiv0{\cdot}24$		$\equiv0{\cdot}16$		$\equiv0{\cdot}96$	$\equiv0{\cdot}1$			
$S\ \mu V/°C$	-28	-23	$+3$	-7	-13	$+30$			
$\chi_M^{300°K}$									
($\times10^{-6}$)	$+4000$	900	40	170	180	$630_{(406°K)}$		200	(very
$T_{N/C/d}$ °K	(C) 120°	(N) 90°	(N ?) 155°		(N) 145°	(d) 341°	(C) 394°		low)
T_S °K	—	—	1·5°	—	7°	—	—	—	—
Plasma edge	0·9 ev		~1·6 ev		1·0 ev	1·4 ev			2·0 ev

† A recent band structure calculation for ReO_3 by L. F. Mattheis, *Phys. Rev.*, 1969, **181**, 987 puts the width of the carrier holding d-band in that case at 2·5 to 3 ev.

pyrite lattice constant shows a marked peak at NiS_2. This would seem to be absent for the selenides, and could well be an indicator of the quasi-ionic localized character of the electrons close to NiS_2, where the e_g* band is in the half-filled condition. The semiconductivity and paramagnetism could arise from a breakdown in band behaviour under high correlation at this point. The very high value of θ_P ($\sim -750°K$), and the low value of χ and p_{eff} (2·48 in place of 2·83 ideally, or 3·2 more typically for the Ni^{2+} ion) are characteristic of materials leaving the ionic regime, cf. NiO, NiI_2, NiS, Cr_2S_3, $TiBr_3$, TiI_2. An examination of the electrical properties of NiS_2 under pressure would be interesting. Of course it is possible that under the action of the crystal field in the somewhat distorted octahedra of the pyrite structure a normal band gap opens up in the e_g* band. This, however, would leave the magnetic properties unexplained.

Fig. 91

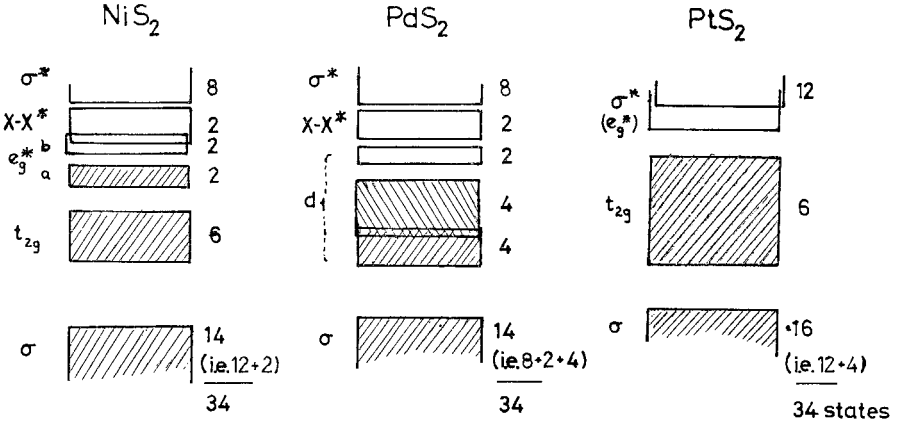

Possible banding arrays for the triplet of group VIIIc semiconductors NiS_2, PdS_2, PtS_2.

Such a band gap does provide a satisfactory account of the diamagnetic semiconducting behaviour of PdS_2 and $PdSe_2$. Here the pyrite structure has been quite severely distorted by elongation along one of the cube axes (see fig. 11). Figure 91 contrasts the proposed banding diagrams for the triplet of VIIIc semiconductors NiS_2, PdS_2, PtS_2. A second form of PdS_2, reverting towards a pyrite structure, is obtained under high pressure, in which the *a* and *b* axes are expanded somewhat and the *c* axis is contracted by almost $\frac{1}{2}$ Å (Munson and Kasper 1969). The metallic nature of this form contrasts with the high resistivity and Seebeck coefficient of the normal semiconducting form ($E_g^{elec} \sim 0{\cdot}8$ ev—Hulliger 1965). Semiconductivity

and diamagnetism is also surprisingly obtained in the rather complex low temperature structures of the group VIIIb materials $IrSe_2$, $RhSe_2$, IrS_2. This contrasts strongly with the metallic character of the rest of group VIIIb, including the alternative pyrite forms of $RhSe_2$ and IrS_2. The $IrSe_2$ structure is built on units of the marcasite structure, and the semiconductivity seems to result from the stacking break of the anion layers (see fig. 10), resulting in fewer X–X pairs than would otherwise occur. Orbitals then drop from the X–X* band and absorb the surplus electrons into the valence bands. The straight group VIIIb marcasite $CoSe_2$ is a metal (Ramdohr 1955).

The marcasites of group VIIIa (viz. $FeS_2/Se_2/Te_2$) are small gap semiconductors similar to the corresponding pyrites. There is still an X–X pair per unit, and the two band structures are likely to be similar, with 14 deep valence electrons and six in the non-bonding t_{2g} band. In the marcasite structure the octahedra share a couple of edges (see fig. 8), rather than being linked by the corners as in the pyrite form, with the result that rows of metal atoms are formed parallel to c as in the rutile structure (fig. 73). When one electron is removed from the t_{2g} band (as in FePS or $CoAs_2$—Hulliger and Mooser 1965) metal–metal *pairing* occurs in this chain yielding the distorted arsenopyrite structure ($E0_7$). The semiconductivity and diamagnetism here resemble that of low temperature VO_2. When two electrons are removed, as in RuP_2 (isoelectronic with MoS_2), the marcasite structure shows a *regular* contraction parallel to c, and semiconductivity again results. The same occurs for $CrSb_2$, where now only the lower third of the non-equivalent t_{2g} states are occupied. With yet two fewer electrons again, as in TiP_2, we obtain a metallic $PbCl_2$-like material, and not an insulating marcasite or pyrite (at least not at normal pressure), despite the precedent of the pyrite SiP_2.

In general the properties of the pnictides are likely to be more difficult to interpret than those of the corresponding chalcogenides, because of the smaller energy separations and the more general state mixing. In their band structures of the three rocksalt materials TiO, TiN and TiC, Ern and Swittendick (1965) show the sort of progression in mixing to expect.

9.2. *The Development of Crystal Structure through the Transition Metal Dichalcogenides*

In the above sections we have dealt with most of the transition metal dichalcogenides and noted how the structure type moves from layered structures, first regular, then distorted, through to marcasite and pyrites, finally to return via the intermediates $IrSe_2$ and PdS_2 to the flattened layer structures like PtS_2. The movement is influenced by both group number and period number—that is, electron configuration and atom size. By looking at the structure parameters in detail we can study these changes more closely.

Fig. 92

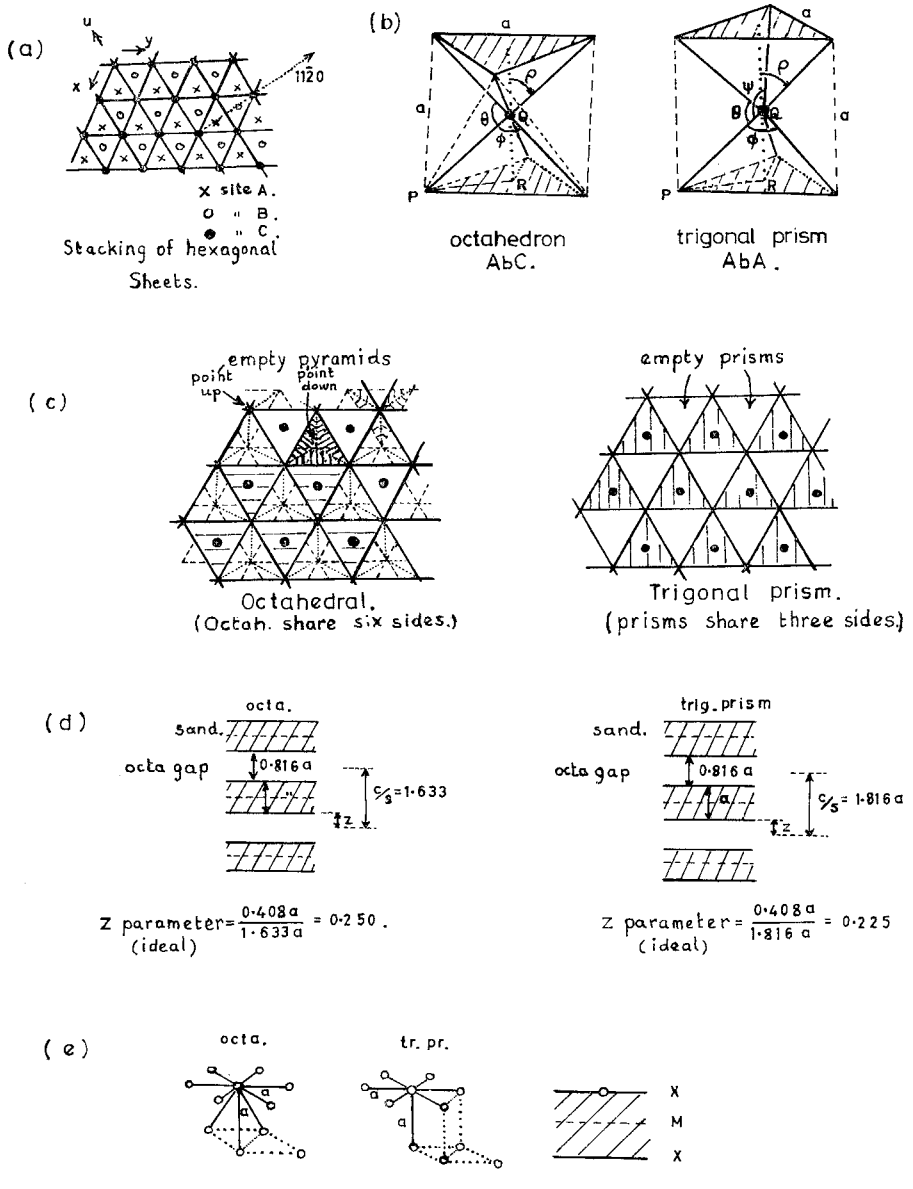

Comparison of the geometry of the ideal octahedral and trigonal prism TX_2 layer structures.

Table 18. Comparison of the geometry of the ideal octahedral and trigonal prism TX_2 layer structures (see fig. 92)

	Octahedron		Trigonal prism
(*a*) With common lattice constant a. All coordination unit sides $=a$			
Bond length	$B_0=0{\cdot}707a$	$<$	$B_p=0{\cdot}763a$
Unit height	$h_0=0{\cdot}816a$	$<$	$h_p=a$
Unit volume	$V_0=0{\cdot}471a^3$	$>$	$V_p=0{\cdot}434a^3$
Coordination units as fraction of sandwich	$\frac{2}{3}$	$>$	$\frac{1}{2}$
Gap height	$g_0=h_0=0{\cdot}816a$	$=$	$g_p=g_0=0{\cdot}816a$
Cell parameter	$c_0=1{\cdot}633a_0$	$<$	$c_p=1{\cdot}816a_p$
(*b*) With common bond length of $0{\cdot}763a_p$			
Lattice constant	$a_0=1{\cdot}08a_p$	$>$	a_p
Unit height	$h_0=0{\cdot}882a_p$	$<$	$h_p=a_p$
Gap height	$g_0=h_0=0{\cdot}882a_p$	$>$	$g_p=h_0'=0{\cdot}816a_p$
$c_0=h_0+g_0$	$=1{\cdot}764a_p$	$<$	$c_p=h_p+g_p=1{\cdot}816a_p$
(*c*) Angles in structure			
(i) In coordination unit			
$\angle$ XMX, θ and $\phi=90°\ 00'$ (12)		$>$	$81°\ 47'$
$\angle$XMX, $\psi=180°\ 00'$ (3)		$>$	$135°\ 35'$ (fig. 92 (*a*))
$\angle$ *z*MX, $\rho=54°\ 45'$		$<$	$49°\ 07'$
(ii) In gap, octahedral sites			
$\angle$ *z*OX, $\delta=54°\ 45'$		$=$	$54°\ 45'$
(*d*) Number of X–X close neighbours within single sandwich			
9 (i.e. 6+3) at a		$>$	7 (i.e. 6+1) at a (fig. 92 (*d*))
(*e*) Further parameters			
(i) z (taken from middle of gap)			
$0{\cdot}250$		$>$	$0{\cdot}225$ (fig. 92 (*c*))
(ii) $\chi=\frac{\text{X–X measured across gap}}{\text{X–X standard v.d.W.}}$			Standards S 3·7 Å Se 4·0 Å Te 4·4 Å

First we shall look at the changes which occur in the layer structures of groups IV, V, VI and VII. The parameters were collected in tables 2 and 3. These should be compared with the ideally coordinated situation, as represented in table 18 and fig. 92. As is seen in part (*a*) of this table, for a common lattice constant a, the bond length is shorter with the octahedral coordination than for the trigonal prism. Since the bond length is of primary energetic importance, part (*b*) of the table shows the data converted to a common bond length. Under these conditions the octahedral a parameter is the greater of the two by about 8%. We begin by comparing materials which exist in both octahedral and trigonal prism forms. The a parameters of 1T–TaS_2 and $TaSe_2$ are indeed found to be greater than

those of the trigonal prism forms (e.g. 2H, 3R), but in fact by only 1%. As mentioned in § 8.2, a refined structure analysis of the 1T materials is not available, but for the trigonal prism tantalum materials it is known that a is greater than for ideal coordination (from the angles X–M–X). Furthermore, in the octahedral 1T forms the very large values of c/a might indicate that there a is a little less than ideal.

Fig. 93

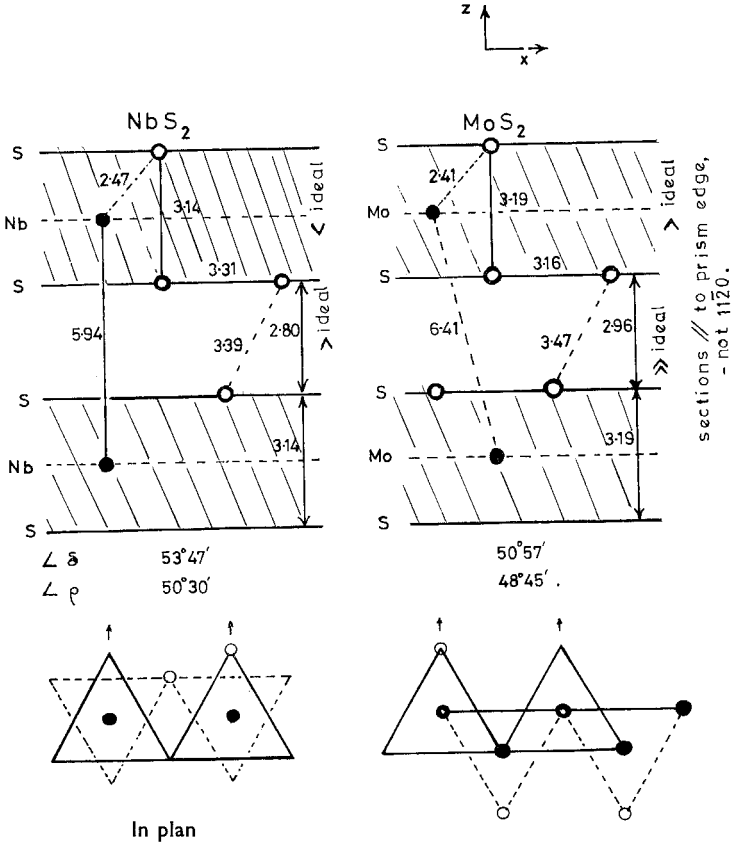

A comparison of the structure deformations in 2H–MoS_2 and 2H–NbS_2. (Note not 11$\bar{2}$0 sections.)

A major cause in the build up of the c/a ratios above ideality is likely to be 'c' expansion due to the repulsive X–X interaction between the top and bottom layers of each individual MX_2 sandwich. This is seen by noting that

(i) c/a for Ti > Zr or Hf materials; also for VSe_2 > 1T–$TaSe_2$,

(ii) c/a for all tellurides > corresponding selenides > sulphides.

i.e. the bigger the X atoms in proportion to the M atom, the bigger is the value of c/a for the resulting structure. From the existing trigonal prism data of table 2 it is seen that both the sandwich coordination units and also the van der Waals gap heights are likely to follow these same sequences, e.g.

	MoS_2	α-$MoTe_2$	
Unit $\angle\rho$	48° 45′	48° 15′	(A smaller angle means
Gap $\angle\delta$	50° 57′	50° 29′	greater elongation $\|\|c$)

Unfortunately no refined data are available for the group IV materials, other than TiS_2. The increase in the *gap* elongation on passing from sulphide to telluride is likely to occur as a reaction to the relative reduction in a. Actually this 'riding up' effect appears to be somewhat offset by a second effect. The van der Waals force parameter χ shows in fact that the attractive force across the gap is a little *stronger* in proportion in the telluride than in the sulphide. The latter effect presumably arises because the interacting X-sheets are individually packed more densely in the telluride than in the sulphide. Figure 14 shows the interesting results obtained by plotting c/a for all these compounds against the separation between the outer electrons of neighbouring X-atoms in such a sheet. Effective orbit radii for this purpose are drawn from Slater (1965, p. 103). The plot reveals the much greater distinction that exists *between* the groups of the Periodic Table than within them. The following data make the contrast between group IV and group V:

	a	c	c/a	Atomic radii of metal
$HfSe_2$	3·75	6·16	1·643	1·59 Å
	↑	↓		↑
1T–$TaSe_2$	3·48	6·27	1·804	1·46
.....	↓	↑		≈
$TiSe_2$	3·53	6·00 Å	1·698	1·47

The expansion in the value of the c parameter of 1T–$TaSe_2$ is not solely an atom size effect, as is seen from the comparison with $TiSe_2$. It is also the product of the single non-bonding electron of 1T–$TaSe_2$ lying in the orbital, shown in fig. 25 (b), where the horizontal lobes force the X-atom sheets apart. In β-$MoTe_2$ and $ReSe_2$, with two or three non-bonding electrons respectively, the averaged value of c/a rises to over 1·9. It is to be remembered that these two materials are in addition distorted somewhat by metal–metal bonding in the layers, as also are the group V tellurides. The effective anisotropy in these compounds due to the

contraction in the chains (measured by the ratio of '$a_{\text{effective}}$' taken perpendicular and parallel to the chains) is for $NbTe_2$ 2·5%, for WTe_2 3·8%, and for $ReSe_2$ 11·5% (see fig. 72)†.

It is also noteworthy that the octahedral and trigonal prismatic forms of TaS_2 and $TaSe_2$ are more closely similar in c/a ratio, than are the trigonal prism compounds of group V to those of group VI. Indeed it seems that the 1T forms pass over smoothly into the 2H, 3R and $4H_a$ forms via the intermediate $4H_b$ and 6R, where octahedral and trigonal prismatic coordination coexist (see p. 302). Figure 93 outlines the marked change in shape which occurs between 2H–NbS_2 (group V) and 2H–MoS_2 (group VI). When it is recalled that, for 'ideal' trigonal prism coordination, the height of the coordination unit and the van der Waals length should both equal the lattice parameter, it is seen that the MoS_2 coordination unit is somewhat extended $\|c$, particularly relative to that of NbS_2. In fact the group V value is below 'ideal', so accounting for the affinity to the 1T form. Further, in MoS_2 the van der Waals length is seen to be very large in comparison to a, though the absolute value of this length remains less than 'standard' (see χ parameter, table 2). The elongated character of $MoS_2/Se_2/Te_2$ is in part due to the very small size of the molybdenum atom; indeed it is one of the smallest atoms to form a layered chalcogenide. The plot of fig. 14 reveals the highly compacted character of the sandwiches, for α-$MoTe_2$ in particular. A second factor causing elongation parallel to c in the MoS_2 family is the action of the filled non-bonding d_{z^2} orbital (see fig. 25), pushing the X-atom sheets apart. Conversely in NbS_2 this orbital is only half-filled, and the relative contraction of the sandwich and gap in this case may be in part due to intersandwich bonding. Indeed in several of the group V polytypes there is a tendency for the metal atoms to line up parallel to c, which is not shown in the two group VI polytypes—see fig. 3. (N.B. 3R is only metastable for group V.)

The very large value of c/a for α-$MoTe_2$ marks the limit for the regular structures, and the value is relaxed somewhat in the distorted octahedral layer structures of β-$MoTe_2$, WTe_2, and the technetium and rhenium compounds. It has been reported that a pyrite form of ReS_2 also exists. The lattice parameter at 5·57 Å is a little smaller than that of OsS_2, and a whole $\frac{1}{2}$ Å smaller than that of MnS_2, indicating that it does not share the quasi-ionic character of its 3d analogue. In the pyrite structure the coordination octahedra are linked by the corners only, with the metal atoms falling on a regular three-dimensional face-centred cubic array (fig. 7). This produces a much denser structure in general (Mn compounds excluded) than does a layer type arrangement, with its 'wasted' van der Waals space. The arrangement of octahedra to achieve the pyrite packing necessitates close X–X approaches, so that the manganese compounds in particular

† N.B. A comparison between $TiTe_2$ and $TaTe_2$ quickly reveals the contraction present in the latter which is absent from the selenide. As mentioned in § 8.2 the structure of 1T–TaS_2/Se_2 is a little strange, but it retains a much higher degree of pseudo-hexagonal symmetry than does the telluride.

finish by resembling the NaCl structure (shown by α-MnS), with the X–X pairs acting as a divalent group. In all three manganese dichalcogenides the X–X distance is very close to that in the elementary form of the respective chalcogen. Such pairings could well contribute 50 kcal/mole (> 2 ev) to the total binding energy. Similar pairings are also present in marcasite (where the octahedra share edges) and in the $IrSe_2$ structure. Table 5 shows how towards the edge of the non-layered domain—as defined by table 15 (*b*)—the X–X pairings are weakened, to allow a material like $RhTe_2$ to move through to the cadmium iodide structure (contrast $RuTe_2$).

The *layer* compounds of group VIII all have in common a very low value of c/a. In PtS_2, for example, although the platinum atom is the same size as the molybdenum atom, the a parameter is 10% greater than for MoS_2. The sandwich flattening in PtS_2 is likely to result from the completely filled non-bonding d orbitals. The tilted lobes of these orbitals lie closer to the c axis than do the bonding orbitals (see fig. 25), so forcing the latter to splay out somewhat. The two sulphur planes of each sandwich now lie closer together, to produce S–S distances *through* the sandwich that are quite small (3·06 Å, as compared with 3·19 Å for MoS_2). This is reminiscent of the behaviour in the pseudo-layer structure of PdS_2 (see fig. 11) where this distance has shrunk to 2·13 Å. The gap height also in PdS_2 is only 2·6 Å compared with 2·75 Å in PtS_2. The van der Waals gap parameter χ for PtS_2 is quite high at 0·93, but because of the large value of a angle δ appears rather large. However, as one goes to the selenide and telluride the gap contracts strongly. Indeed all the group VIII tellurides have a gap height of only about 2·5 Å as compared with 3·35 Å in α-$MoTe_2$†. The metallic properties of Pt/Pd/$NiTe_2$ indicate that the conduction band is overlapping the d bands, and the energetics of the situation are far from simple. Structure determining factors are in general known to be a very small fraction of the total energy locked in any compound, as the heats of formation of polymorphic forms reveal.

Finally we return to groups V and VI to mention the only transition metal dichalcogenides not to exist—viz. VS_2 and $CrS_2/Se_2/Te_2$. (N.B. the pyrite RhS_2 is very metal deficient.) Chromium and vanadium form a whole series of chalcogenides (see Jellinek 1963), e.g. M_5X_6, M_3X_4, M_2X_3, converting a NiAs-type structure through towards a CdI_2 type (see fig. 15) by the progressive abstraction of metal atoms from alternate metal sheets. However, the most chalcogen rich products obtained, even under high pressure, have only the composition M_5X_8 (Sleight and Bither 1969). The

† PtS_2 displays a very large disparity in expansion coefficient ∥ and ⊥c

Expansion coefficients		PtS_2	$PtSe_2$	$PdTe_2$	CdI_2	
α	∥c	37	20	30	40	
	⊥c	2·3	5·7	12	10	$\times 10^{-6}\,°C^{-1}$

(Kjekshus and Grønvold 1959).

effective c/a ratio of Cr_5Se_8, reckoned as a non-stoichiometric layer structure, is 1·605, the very low value of which is an indication as to why the end product $CrSe_2$ does not form†. Certainly a nominal valency of 4 for chromium is not impossible, as CrO_2 shows. This latter compound is a rutile, and closely similar to MoO_2, but without the metal–metal bonding of the latter. '4' is of course a more acceptable valency for molybdenum, and MoS_2 forms its natural ore, 'molybdenite'. The stability of Cr_2S_3 relative to the instability of Mo_2S_3 underlines the preference of chromium for trivalency. This also serves to explain why pressure does not lead to production of a pyrite form of CrS_2. The pseudo-divalency required for the pyrite form is not in line with the high degree of s–d mixing still present in chromium compounded with a chalcogen. Divalency can be induced by chlorine, and $CrCl_2$ forms as a Jahn–Teller distorted marcasite (Tracy *et al.* 1961). The absence of Jahn–Teller type distortion in the octahedra of the pyrite and marcasite structures of the d^7 cobalt dichalcogenides of course underlines that these chalcogenides are not ionic in the standard sense, there being a fair degree of d mixing into the valence band as discussed in § 9.1. $MoCl_2$ is again quite different from $CrCl_2$, being a distorted layer structure, and without ligand field spectra (Clark 1964). The layer halides will be discussed in the next section, but the plot of fig. 14 shows how similar the simple ionic dihalide structures are irrespective of group number—in sharp contrast to the dichalcogenides.

9.3. *Survey of the Properties of the Layer-type Transition Metal Halides*

The majority of the transition metal *di*halides (in anhydrous form) adopt the layer structure of $CdCl_2$ or CdI_2‡. As seen earlier all the *layered* dichalcogenides are of covalent rather than ionic character, i.e. they do not show the low intensity many-electron d state 'crystal field' spectra, are not salt-like paramagnetics, and in appropriate cases exhibit metallic conduction. Among the dihalides, however, compounds such as $CoCl_2$, $MnCl_2$ and VCl_2 are all typically salt-like by such criteria. Furthermore, they show the long 'bond' lengths typical of ionic materials (e.g. $CoCl_2$, experiment 2·52 Å, sum of atomic radii 2·35 Å—Slater 1965, p. 308ff). The *pyrite* dichalcogenides are intermediate between these groups, MnS_2 being salt-like, but CoS_2 showing delocalization and metallic properties. As in the monoxide and monosulphide families the greatest degree of localization is to be expected for manganese, this tendency decreasing towards the edges of the period (3d), viz. towards nickel and particularly towards titanium. The origins of this effect were discussed in § 5.1. Indeed the superconducting metallic properties of TiO (Denker 1964) tempt one to look at $TiCl_2/Br_2/I_2$ for possible metallic properties, whilst the metal/insulator

† c/a for the isostructural V_5Se_8 is 1·715, and VSe_2 goes on to form with $c/a = 1{\cdot}82$ (Røst and Gjertsen 1964). In these T_5X_8 products the metal deficient sheets are only one-third full.

‡ Excluding the fluorides.

Fig. 94

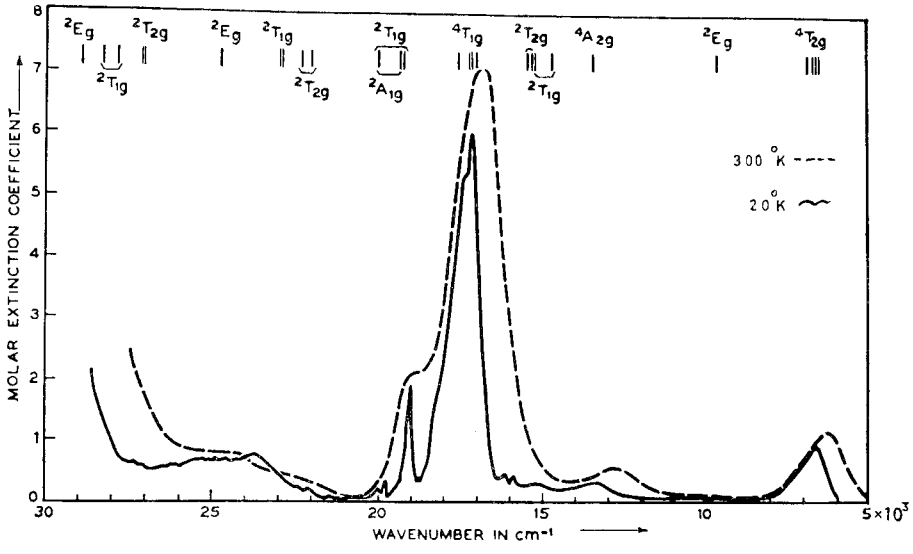

Ligand field spectrum of $CoCl_2$. (Ferguson *et al.* 1963.)

transition in NiS (Sparks and Komoto 1968) and also possibly NiS_2 point to $NiCl_2/Br_2/I_2$ as an interesting series. What data there are at present available supports this. The following table shows the run of the bond length and susceptibility criteria through the nickel halide series.

	Ni–X distance		$\chi^{300°K}$ Molar (c.g.s.)	Colour
	Experiment	Atom sum		
$NiCl_2$	2·51	2·35	6150	Yellow
$NiBr_2$	2·64	2·50	5600	Brown
NiI_2	2·78	2·75 Å (ref. above)	3880×10^{-6}	Black

The melting point of these nickel halides is also 300°c higher than those of the corresponding manganese, iron and cobalt salts. The ligand field spectra of the latter halides have been reported in several papers (see Hush and Hobbs 1968) and show nothing like the red shift and gain in intensity for these transitions that is found in the nickel case (see fig. 95). This is reminiscent of the behaviour observed in the series MnO/MnS/MnSe (Lohr and McClure 1968), or the layer compounds $CrCl_3/Br_3/I_3$ (Dillon *et al.* 1966).

Fig. 95

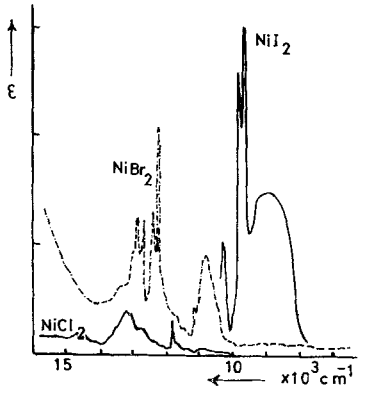

Ligand field spectra of $NiCl_2$, $NiBr_2$ and NiI_2 (as the gaseous TX_2 linear molecule species). (De Kock and Gruen 1967.)

The Néel point in TiI_2 (d^2) appears to be in the region of 200°K and the susceptibility is of low magnitude ($\sim 1800 \times 10^{-6}$ c.g.s./mole at 300°K—Klemm and Grimm 1942 b—compare for the $(d\gamma)^6 (d\epsilon)^2$ Ni^{2+} ion in $NiCl_2$ above, where the value is much higher). For $TiCl_2 T_N$ is reported as 85°K (Lewis *et al.* 1962). Such values should be compared with $MnCl_2$ 2°K, $CoCl_2$ 25°K, $NiBr_2$ 60°K (collected data, Goodenough 1963). Both TiI_2 and $TiCl_2$ are black with high continuous absorption in the photon energy range 1 to 4 ev (Clark 1964). We intend to investigate these compounds directly and under pressure to see whether they exhibit metallic properties above or below the Néel point. If they are metallic only above this temperature they would resemble α-NiS; if metallic only below this temperature they may provide the first clear cut example of a Mott-type insulator to metal transition. In these compounds where band formation is in a critical stage the effect of pressure could be very marked (cf. $MnTe_2$—see § 9.1). Pressure has been shown (via detailed analysis of the ligand field spectra—Zahner and Drickamer 1961) to increase the degree of covalency in the salts $MnCl_2$, $NiCl_2$, etc.

In VCl_2 the d overlap is less than for $TiCl_2$ (cf. VO versus TiO) and ligand field spectra are obtained from the pale yellow crystals (Clark 1964). Crystals of VBr_2 are red, and of VI_2 again black†, following the covalency rise. The covalency rise on moving to the 4d zirconium dihalides is matched by a marked drop in susceptibility to $\sim 150 \times 10^{-6}$ c.g.s. units/mole (Lewis *et al.* 1962). This is less than that of NiS ($\sim 220 \times 10^{-6}$ c.g.s. units/mole—Sparks and Komoto 1968). As always in these cases of incipient band formation, there is at the moment some doubt concerning the stability of the regular structure (Klemm and Grimm 1942 a), but an electron diffraction

† Two forms exist for VI_2, black and red (Juza *et al.* 1969), but the structural difference is slight and as yet undetermined.

pattern would readily detect a distortion of the type found in β-$MoTe_2$ (also with 18 valence electrons). Many of the 4d and 5d dihalides, such as $NbCl_2$, $MoCl_2$, WI_2, $PdCl_2$, do indeed have more complex structures than their 3d counterparts, so denying simple comparisons (Canterford and Colton 1968).

An interesting comparison can be made between VBr_2 and VSe_2, both CdI_2-type materials. The former is salt-like, the latter a metal. The metal–metal spacings in the sandwiches are 3·77 and 3·35 Å amounting to 41 and 25% increases respectively on the spacing in elemental vanadium. These percentages should be compared with the following:

MnI_2	NiI_2	VI_2	TiI_2	Zr/Nb/$MoTe_2$	Zr/Nb/MoS_2	MnS_2	FeS_2[P]	FeS_2[M]
65	56	54	40	25	14	71	52	34%

Of course the non-metallic properties of VBr_2 are not just induced by the larger metal atom separation, but also by the more electronegative role of the halide ligand in causing d shell contraction (see § 5.1). The band properties apparent in the pyrites FeS_2, CoS_2, etc. emphasize moreover, that the formation of these bands, though prominently based on the metal d states, is mediated to some extent by the chalcogenide states.

Such mixing is dependent on the basic $\sigma\sigma^*$ ('charge transfer') energy. We can get a fair idea of what energies of this kind will be from the spectra of the corresponding manganese and zinc compounds, where d transitions are either weak or absent, e.g.

MnS/ZnS, $E_g \approx 3{\cdot}9$ ev; (Ford *et al.* 1963)	MnI_2/ZnI_2, $E_g \approx 3{\cdot}2$ ev; (Tubbs 1968)	MnS_2/ZnS_2, $E_g \approx 3$ ev. (Bither *et al.* 1968)

For $ZnCl_2$, $E_g \sim 7$ ev, and so throughout the transition metal dichlorides halide mixing with the metal states will be at a minimum. Hence our interest in possible isolated d band metallic properties for $ZrCl_2$, etc. It is not only the dihalides but also the tri-halides of group IV which offer interesting possibilities in this respect.

The metal–metal spacing is only a little closer (3·555 Å versus 3·561 Å) in α-$TiCl_3$ than in the divalent $TiCl_2$. No refined data are available on the Ti–Cl bond lengths. α-$TiCl_3$ has the 'honey-comb' metal layer sandwich structure shown in fig. 96 (*a*). With one non-bonding electron per metal atom it is in a condition deserving comparison with VO_2, $NbSe_2$ or $CoSe_2$. There is a very sharp drop in its susceptibility occurring at 217°K (Ogawa 1960). Just above this temperature χ reaches a value of 1100×10^{-6} c.g.s. units/mole—a fairly salt-like value (cf. $\chi_M{}^{300°}$ for the more ionic TiF_3 (d^1) and $Cu(NO_3)_2 . 6H_2O$ ($d^9 \equiv d^1$) of 1300×10^{-6} and 1625×10^{-6} respectively);

Fig. 96

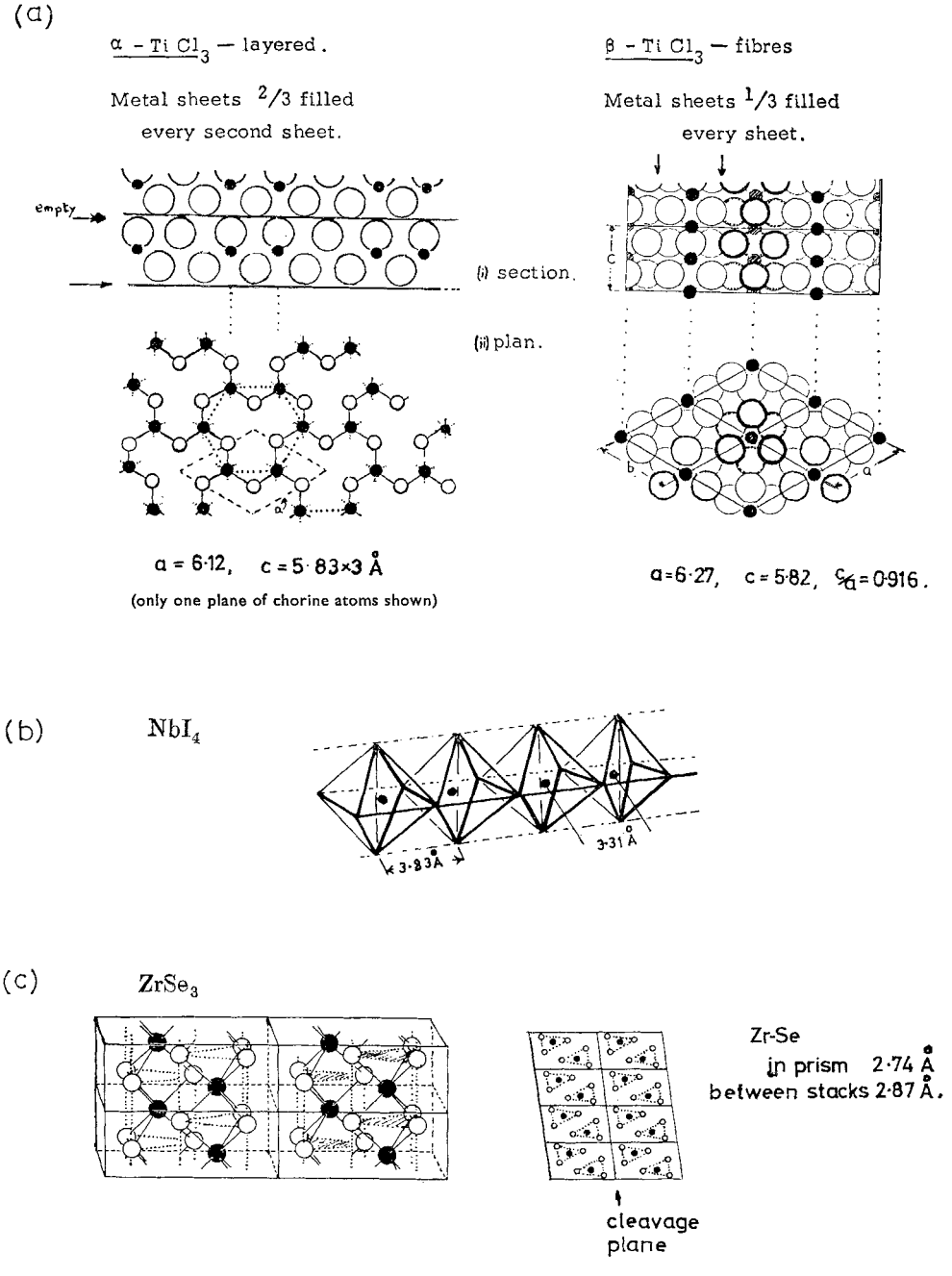

Crystal structures of the linear chain compounds. (*a*) β-TiI_3, based on Dahl *et al.* 1964. (*b*) NbI_4, based on Dahl *et al.* 1962. (*c*) $ZrSe_3$, based on Kronert and Plieth 1965.

below 217°K, χ for α-$TiCl_3$ quickly drops to one-tenth the value. For further comparison the peak susceptibilities of some 'one-electron' *band* compounds are for $CoSe_2$ (90°K) 1400×10^{-6}, for VO_2 (340°K) 700×10^{-6}, and for $NbSe_2$ (160°K) only 200×10^{-6}. From optical absorption (Baldini *et al.* 1968) it would seem that α-$TiCl_3$ is an insulator both above and below the discontinuity temperature, since the single ligand-field peak of the d^1 'ion' is seen in both ranges. Infra-red, pressure and conductivity measurements at low temperatures would be valuable. There is also a possibility of structure distortion below T_d—certainly the volume contracts by almost 2% (Ogawa 1960)—a value equal but *opposite* to that in NiS (Sparks and Komoto 1963).

Again the materials tend to opt out of this critical condition by adopting an alternative structure. β-$TiCl_3$ has the very interesting structure shown in fig. 96 (*a*). It seems that this is the normal form adopted by TiI_3 and the Zr and Hf trihalides (Dahl *et al.* 1964). All these β materials appear at first sight to have the possibility of being metals as they show low constant paramagnetism $\sim 200 \times 10^{-6}$ c.g.s./mole (Lewis *et al.* 1962, Llemm and Krose 1947) and no longer exhibit the ligand field peak (Clark 1964, Baldini *et al.* 1968). Indeed it is possible in the Zr and Hf compounds that absorption is rising into the infra-red, as if from free carriers (Schläfer and Wille 1967). No electrical or optical absorption measurements on single crystals have as yet been made. As is seen from fig. 96 (*a*) the β-$TiCl_3$ structure consists of 'independent' linear stacks of face-sharing octahedra, and this raises the interesting possibilities of linear chain metals in general. In particular superconductivity may occur at highish temperatures (see Dzyaloshinskii and Katz 1969—contrast Ginzburg 1968, p. 367 ff). (β)-HfI_3 would seem to offer an excellent chance for linear chain metal behaviour, since the metal–metal distance in the chains at 3·3 Å is only 0·1 Å larger than the distance in hafnium metal itself. Indeed in $ZrCl_3$ this distance is $\sim 0{\cdot}1$ Å *shorter* than in the element. There are, however, some slight indications of metal–metal bonding and a superstructure forming within the chains (Struss and Corbett 1969, Watts 1966, Schnering 1966). In NbI_4 and TaI_4, where chains of octahedra share edges, the metal atoms are definitely grouped in displaced pairs (fig. 96 (*b*)), but there (as with l.t. VO_2) the compound is diamagnetic Schnering 1963). In the $ZrSe_3$ family, where we have stacks of trigonal prisms (fig. 96 (*c*)), we again end with diamagnetic semiconductors (McTaggert and Wadsley 1958, Kronert and Plieth 1965) due to some cross-linking between the stacks. Hence the β-$TiCl_3$ family could possibly stand in a unique position.

We do not wish to enter into further discussion of these halides until our experimental work on these systems is more advanced, but the above survey does serve to show in what manner the halides usefully complement the chalcogenides in any investigation of bonding and banding in transition metal compounds. On the experimental and practical side, however, there is one great disadvantage that the halides suffer relative to most of the chalcogenides. They are extremely susceptible to chemical attack by moist air.

§ 10. Summary and Conclusion

Our own experimental work has been based on optical studies of the MoS_2 type layer dichalcogenides. Because of the unique properties of such structures we automatically have taken an interest in layer materials in general. Further, since the layered dichalcogenides like ZrS_2, NbS_2, MoS_2, ReS_2 and PtS_2 show a wide range of electrical and optical properties of the narrow d band type, we have also looked in this paper for comparisons with the neighbouring non-layered transition metal dioxides (e.g. TiO_2, VO_2, CrO_2) and dichalcogenides (e.g. MnS_2, FeS_2, CoS_2, NiS_2). Both halves of the dichalcogenide family, layered and non-layered, have much in common and take up an interesting position in the general progression of transition metal compounds. This progression is one of d state participation in crystal binding and band formation. The dichalcogenides fall between the 'ionic' localized d state materials such as the halides and oxysalts on the one hand, and the binary 'alloy materials' such as CrSb, V_3Si or $MoAl_2$ on the other. In fact they just span the critical overlap condition for d band conduction, $MnS_2/Se_2/Te_2$ alone behaving quasi-ionically. NiS_2 seems to sit right on the dividing line. In CoS_2/Se_2 and VSe_2 overlap conditions are just sufficient to allow itinerant band magnetism to develop. In the layered NbS_2 family band antiferromagnetism occurs along with superconductivity (cf. M. H. Cohen 1967). $CuSe_2$, $RhSe_2$, β-$MoTe_2$, $PdTe_2$ are among the other superconductors.

Much theoretical effort has of late gone into describing the narrow d band condition and incipient band formation, via the Hubbard Hamiltonian and the strong correlation problem (see Kemeny, Arai, Caron, etc. Int. Conf. on Metal/Non-metal Transition, *Rev. mod. Phys.*, **40**, No. 4 (Oct. 1968)). Two simpler effective one-electron descriptions of this complex situation have been developed at M.I.T. and by J. C. Slater's group (see Adler and Feinleib 1969—NiO; T. M. Wilson 1969—MnO). Slater's spin-polarized A. P. W. procedure (Slater 1968) in a case like that of MnO will allow a good estimate to be obtained of the ligand field d–d transition energies. The method is identical with that used on magnetic metals, e.g. ferromagnetic Ni (Connolly 1967) and antiferromagnetic Cr (Yamashita *et al.* 1968). It would be very interesting to see a calculation of this type made for the band antiferromagnets like NbS_2, particularly in view of their superconducting properties. A recent paper by Rice *et al.* (1969) has stressed the formal similarity in the theories of band antiferromagnetism and superconductivity.

Temporary band models for the TX_2 layer compounds have been produced above, which explain satisfactorily the present optical and electrical data. These involve fairly 'pure' d bands with widths ranging from 0·4 to 2 ev. The models were derived with the aid of the chemical bond molecular orbital approach. Indeed a more localized valence band model is now receiving considerable attention from theoretical physicists (see Anderson 1968, Jarós 1968, Heine and Jones 1969).

A most interesting feature of NbS_2 is its intimate relation to the semiconductor MoS_2 (cf. CoS_2, which is a metal, relative to FeS_2, which is a

semiconductor). Complete solid solution between the two allows the electron concentration to be manipulated at will, and offers wide scope to the magnetic and superconducting properties. The very strong excitonic features in the optical absorption spectrum of MoS_2 have been observed under conditions of controlled screening via Nb doping. The excitons in pure MoS_2 have rather large binding energy ($\sim 0{\cdot}05$ ev) and are very temperature stable. Remanent humps even occur in the spectrum of NbS_2. Indeed it is possible that the excitonic interaction may contribute to the cause of superconductivity in these compounds. The Bose-Einstein condensation and superfluidity of excitons seems also to be a possibility for these materials (see Gergel *et al.* 1968). The strongly two-dimensional character of layer crystals adds to the possibility of finding new extremal states of matter.

Perhaps the most unusual material of this family of compounds is the 1T form of TaS_2. This appears to be superconducting and yet possibly not even a semi-metal. β-$MoTe_2$ is similar in being diamagnetic and superconducting, but is definitely a semi-metal, although the free-carrier absorption does not start until well into the infra-red. A preliminary investigation of 1T–TaS_2 would seem to indicate a much smaller lattice distortion than that of β-$MoTe_2$, and one moreover which appears incommensurate with the basic lattice. It is just possible that the state may arise from an excitonic insulator type of effect, across a small inter d band gap, created when a narrow closed d band falls away from the bulk of empty d states under strong correlation. Certainly, in α-$MoTe_2$, we seem to have a set of bands that will allow the excitonic insulator theory (Halperin and Rice 1968) to be tested at high pressures and low temperatures.

The various stacking polytypes of a given layer compound have interesting small variations in lattice parameter, but unexpectedly large variations can occur in certain other properties, e.g. in group VI, the spin–orbit splitting of exciton states; and in group V, the superconducting transition temperatures. This indicates that there remains considerable interaction between the sandwiches of the layer structures despite the very large electrical and thermal anisotropy in these materials. The same is likely to be true also for a linear chain material like ZrI_3, and indeed such cross intraction is essential if superconductivity is to be found in such a material.

Clearly a considerable amount of effort is likely to be expended in the near future on these materials, the spot light most probably falling on the group V dichalcogenide metals. The group IV layer and chain halides would also look to be a field which could be studied with profit.

Acknowledgments

We would like to thank past and present members of this laboratory for their help and advice. In particular we thank Dr. Connell, Dr. Liang and

Mr. Bromley for allowing us to use their unpublished results. We have benefited greatly from stimulating discussions with Professor Sir Nevill Mott, F.R.S.

References

Abdullaev, G. B., Guseinova, E. S., and Tagiev, B. G., 1967, *Phys. Stat. Sol.*, **20,** 421.

Adachi, K., Sato, K., and Takeda, M., 1969, *J. phys. Soc. Japan,* **26,** 631.

Adler, D., 1968, *Solid St. Phys.*, **21,** 1.

Adler, D., and Brooks, H., 1967, *Phys. Rev.*, **155,** 826.

Adler, D., and Feinleib, J., 1969, *J. appl. Phys.*, **40,** 1586.

Alcock, N. W., and Kjekshus, A., 1965, *Acta chem. scand.*, **19,** 79.

Allen, P. B., and Cohen, M. L., 1969, *Phys. Rev.*, **177,** 707.

Altmann, S. L., and Bradley, C. J., 1967, *Proc. phys. Soc.*, **92,** 764.

Amelinckx, S., 1964, *Phys. Stat. Sol.* suppl., **6,** §10.

Anderson, P. W., 1968, *Phys. Rev. Lett.*, **21,** 13.

Andres, K., Kuebler, N. A., and Robin, M. B., 1966, *J. Phys. Chem. Solids,* **27,** 1747.

Andriyashik, M. V., Sakhnovskii, M., Timofeev, V. B., and Yakimova, A. S., 1968, *Phys. Stat. Sol.*, **28,** 277.

Aoyagi, K., Misu, A., Shinada, M., *et al.*, 1966, *J. phys. Soc. Japan,* **21,** 174.

Appel, J., 1968, *Solid St. Phys.*, **21,** 193.

Arko, A. J., Marcus, J. A., and Reed, W. A., 1968, *Phys. Rev.*, **176,** 671.

Asanabe, S., 1961, *J. phys. Soc. Japan,* **16,** 1789.

Asnin, V. M., and Rogachev, A. A., 1967, *Phys. Stat. Sol.*, **20,** 755.

Asnin, V. M., Rogachev, A. A., and Ryvkin, S. M., 1968, *Soviet Phys. Semicond.*, **1,** 1447.

Au Yang, M. Y., and Cohen, M. L., 1969, *Phys. Rev.*, **178,** 1279.

Baldini, G., Pollini, I., and Spinolo, G., 1968, *Phys. Stat. Sol.*, **27,** 95.

Barinskii, R. L., and Vainshtein, E. E., 1957, *Izv. Akad. Nauk SSSR.* Ser. Fiz., **21,** 1375.

Barker, A. S., Verleur, H. W., and Guggenheim, H. J., 1966, *Phys. Rev. Lett.*, **17,** 1286.

Barricelli, L. B., 1958, *Acta crystallogr.*, **11,** 75.

Barstad, J., Grønvold, F., Røst, E., and Vestersjo, E., 1966, *Acta chem. scand.*, **20,** 2865.

Bassani, F., Greenaway, D. L., and Fischer, G., 1964, *VIIth Conf. on Semiconductors,* Paris, p. 51.

Bassani, F., and Parravicini, G. P., 1967, *Nuovo Cim.* B, **50,** 95.

Bennemann, K. H., Garland, J. W., and Mueller, F. M., 1969, *Phys. Rev. Lett.*, **23,** 169.

Bernard, J., and Jeannin, Y., 1962, Adv. in Chem. ' Non-stoichiometric Compounds ', p. 191.

Birman, J. L., 1962, *Phys. Rev.*, **127,** 1093.

Bither, J. A., Bouchard, R. J., Cloud, W. H., Donohue, P. C., and Siemons, W. J., 1968, *Inorg. Chem.*, **7,** 2208.

Bjerkelund, E., and Kjekshus, A., 1967, *Acta chem. scand.*, **21,** 513.

Bongers, P. F., *et al.*, 1968, *J. Phys. Chem. Solids,* **29,** 977.

Borghese, F., and Donato, E., 1968, *Nuovo Cim.* B, **53,** 283.

Bouchard, R. J., 1968, *Mat. Res. Bull.*, **3,** 563.

Brebner, J. L., and Fischer, G., 1962, *VIth Int. Conf. Semiconductors,* Exeter, p. 760.

Brebner, J. L., and Mooser, E., 1967, *Physics Lett.* A, **24,** 274.

BRIXNER, L. H., 1962, *J. Inorg. nucl. Chem.*, **24,** 257 ; 1963, *J. electrochem. Soc.*, **110,** 289.
BRIXNER, L. H., and TEUFER, G., 1963, *Inorg. Chem.*, **2,** 992.
BROWN, B. E., 1966, *Acta crystallogr.*, **20,** 264.
BROWN, B. E., and BEERNTSEN, D. J., 1965, *Acta crystallogr.*, **18,** 31.
BUSCH, G., FROHLICH, C., HULLIGER, F., and STEIGMEIER, E., 1961, *Helv. Phys. Acta,* **34,** 359.
CANTERFORD, J. H., and COLTON, R., 1968, *Halides of the Transition Elements* (Wiley Interscience).
CHAMBERLAND, B. L., 1967, *Mater. Res. Bull.*, **2,** 827.
CHAMPION, J. A., 1965, *Br. J. appl. Phys.*, **16,** 1035.
CHAMPNESS, C. H., and KIPLING, A. L., 1965, *Can. J. Phys.*, **44,** 769.
CLARK, R. J. H., 1964, *J. chem. Soc.*, p. 417.
CLENENDEN, R. L., and DRICKAMER, H. G., 1966, *J. chem. Phys.*, **44,** 4223.
COHEN, M. H., 1967, *Fermi School Physics,* **37,** 403.
COHEN, M. L., and KOONCE, C. S., 1966, *VIIIth Conf. on Semiconductors,* Kyoto, p. 633. *J. phys. Soc. Japan,* **21,** Suppl.
CONNELL, G. A. N., WIETING, T., WILSON, J. A., and YOFFE, A. D., 1968, *IXth Conf. on Semiconductors,* Moscow, p. 414.
CONNELL, G. A. N., WILSON, J. A., and YOFFE, A. D., 1968, *J. Phys. Chem. Solids,* **30,** 287.
CONNOLLY, J. W. D., 1967, *Phys. Rev.*, **159,** 415.
CONROY, L. E., and PARK, K. C., 1968, *Inorg. Chem.*, **7,** 459.
DAHL, L. F., CHIANG, T. I., SEABURGH, P. W., and LARSEN, E. M., 1964, *Inorg. Chem.*, **13,** 1236.
DAHL, L. F., and WAMPLER, D. L., 1962, *Acta crystallogr.*, **15,** 903.
DAS, D. (now Mrs. Paul), 1968, *Indian J. Phys.*, p. 943.
DEKOCK, C. W., and GRUEN, D. M., 1967, *J. chem. Phys.*, **46,** 1096.
DENKER, S. P., 1964, *J. Phys. Chem. Solids,* **25,** 1397.
DEXTER, D. L., and KNOX, R. S., 1965, *Excitons* (New York : Interscience).
DICKENS, P. G., and NEILD, D. J., 1968, *Proc. Faraday Soc.*, **64,** 13.
DILLON, J. F., KAMIMURA, H., and REMEIKA, J. P., 1966, *J. Phys. Chem. Solids,* **27,** 1531.
DOMINGO, G., ITOGA, R. S., and KANNEWUF, C. R., 1966, *Phys. Rev.*, **143,** 536.
DONOHUE, P. C., SIEMONS, W. J., and GILLSON, J. L., 1968, *J. Phys. Chem. Solids,* **29,** 807.
DZYALOSHINSKII, I. E., and KATZ, E. I., 1969, *Soviet Phys. JETP,* **28,** 178.
ERN, V., and SWITENDICK, A. C., 1965, *Phys. Rev.* A, **137,** 1927.
EVANS, B. L., 1966, *Proc. R. Soc.* A, **289,** 275.
EVANS, B. L., and YOUNG, P. A., 1965, *Proc. R. Soc.* A, **284,** 402 ; 1967 a, *Ibid.*, **298,** 74 ; 1967 b, *Proc. phys. Soc.*, **91,** 475 ; 1968, *Phys. Stat. Sol.*, **25,** 417.
FEINLEIB, J., SCOULER, W. J., and FERRETTI, A., 1968, *Phys. Rev.*, **165,** 765.
FERGUSON, J., WOOD, D. L., and KNOX, K., 1963, *J. chem. Phys.*, **39,** 881.
FILLINGHAM, P. J., 1967, *J. appl. Phys.*, **38,** 4823.
FISCHER, F., 1969, *Phys. Stat. Sol.*, **31,** 601.
FISCHER, D. W., and BAUN, W. L., 1968, *J. appl. Phys.*, **39,** 4757.
FIVAZ, R., 1966, *Helv. Phys. Acta,* **39,** 247 ; 1967, *J. Phys. Chem. Solids,* **28,** 839.
FIVAZ, R., and MOOSER, E., 1964, *Phys. Rev.* A, **136,** 833 ; 1967, *Ibid.*, **163,** 743.
FORD, R. A., KAUER, E., RABENAU, A., and BROWN, D. A., 1963, *Bunsenges,* **67,** 460.
FRANZEN, H. F., SMEGGIL, J., and CONARD, B. R., 1967, *Mater. Res. Bull.*, **2,** 1087.
FRINDT, R. F., 1965, *Phys. Rev.* A, **140,** 536 ; 1966, *J. appl. Phys.*, **37,** 1928.

FRINDT, R. F., and YOFFE, A. D., 1963, *Proc. R. Soc.* A, **273,** 69.
FURUSETH, S., SELTE, K., and KJEKSHUS, A., 1965, *Acta chem. scand.*, **19,** 257.
GAHWILLER, C., and HARBEKE, G., 1968, March. Am. Phys. Soc. Meeting, Berkeley.
GAY, J. G., ALBERS, W. A., and ARLINGHAUS, F. J., 1968, *J. Phys. Chem. Solids,* **29,** 1449.
GELLER, S., 1955, *J. Am. chem. Soc.*, **77,** 2641.
GERGEL, V. A., KAZARINOV, R. F., and SURIS, R. A., 1968 a, *Soviet Phys. JETP,* **26,** 354 ; 1968 b, *Ibid.*, **27,** 159.
GINZBURG, V. L., 1968, *Contemp. Phys.*, **9,** 355.
GOBRECHT, H., SEECK, S., and KLOSE, T., 1966, *Z. Phys.*, **190,** 427.
GOODENOUGH, J. B., 1963, *Magnetism and the Chemical Bond* (Interscience); 1966, *J. appl. Phys.*, **37,** 1415 ; 1967 a, *Mater. Res. Bull.*, **2,** 37 ; 1967 b, *Ibid.*, **2,** 165 ; 1967 c, *Czech. J. Phys.* B, **17,** 304 ; 1968 a, *J. appl. Phys.*, **39,** 403 ; 1968 b, *Phys. Rev.*, **171,** 466 ; 1968 c, *Mater. Res. Bull.*, **3,** 409.
GRAESER, S., 1964, *Schweiz Min. Pet. Mitt.*, **44,** 121.
GREENAWAY, D. L., and HARBEKE, G., 1965, *J. Phys. Chem. Solids,* **26,** 1585 ; 1966, *VIIIth Conf. on Semiconductors,* Kyoto, p. 151.
GREENAWAY, D. L., and NITSCHE, R., 1965, *J. Phys. Chem. Solids,* **26,** 1445.
GRIMMEIS, v. H. G., RABENAU, A., HAHN, H., and NESS, P., 1961, *Bunsenges,* **65,** 9.
GRØNVOLD, F., HAGBERG, O., and HARALDSEN, H., 1958, *Acta chem. scand.*, **12,** 971.
GRØNVOLD, F., and RØST, E., 1957, *Acta crystallogr.*, **10,** 329.
GUGGENBERGER, L. J., and JACOBSON, R. A., 1968, *Inorg. Chem.*, **7,** 2257.
GUGGENHEIM, J., HULLIGER, F., and MULLER, J., 1966, *Helv. phys. Acta,* **34,** 408.
GUSEINOV, G. D., and RASULOV, A. I., 1966, *Phys. Stat. Sol.*, **18,** 911.
HALPERIN, B. I., and RICE, T. M., 1968, *Solid St. Phys.*, **21,** 116.
HALPERN, J., 1966, *J. phys. Soc. Japan,* **21,** 180. (Kyoto Conf.)
HARALDSEN, H., 1966, *Angew Chem.* (int. ed.), **5,** 58.
HARALDSEN, H., GRØNVOLD, F., and HURLEN, T., 1956, *Z. Anorg. allg. Chem.*, **283,** 143.
HARPER, P. G., and HILDER, J. A., 1968, *Phys. Stat. Sol.*, **26,** 69.
HASTINGS, J. M., ELLIOTT, N., and CORLISS, L. M., 1959, *Phys. Rev.*, **115,** 13.
HATTORI, M., ADACHI, K., and NAKANO, H., 1969, *J. phys. Soc. Japan,* **26,** 642.
HEINE, V., and JONES, R. O., 1969, S. 2, *Proc. R. Soc., Sol. Stat. Phys.*, **2,** 719.
HICKS, W. T., 1964, *J. electrochem. Soc.*, **111,** 1058.
HOCKINGS, E. F., and WHITE, J. G., 1960, *J. phys. Chem.*, **64,** 1042.
HOLSETH, H., and KJEKSHUS, A., 1968, *J. less-common Metals,* **16,** 472.
HOLT, S. L., and WOLD, A., 1967, *Inorg. Chem.*, **6,** 1595.
HUFFMAN, D. R., 1969, *J. appl. Phys.*, **40,** 1334.
HUISMAN, R., and JELLINEK, F., 1969, *J. less-common Metals,* **17,** 111.
HULLIGER, F., 1960, *Helv. Phys. Acta,* **33,** 959 ; 1963, *Nature, Lond.*, **200,** 1064 ; 1964, *Ibid.*, **204,** 644 ; 1965, *J. Phys. Chem. Solids,* **26,** 639.
HULLIGER, F., and MOOSER, E., 1965, *Prog. Solid St. Chem.*, **2,** 330.
HULTGREN, R., 1932, *Phys. Rev.*, **40,** 891.
HUSH, N. S., and HOBBS, R. J. M., 1968, *Prog. Inorg. Chem.*, **10,** 259.
HYLAND, G. J., 1968, *Proc. phys. Soc.*, S. 2, 1, 189.
ISKENDEROV, R. N., DRABKIN, I. A., EMELYANOVA, L. T., and KSENDZOV, M., 1968, *Soviet Sol. Stat.*, **10,** 2031.
JAMES, P. B., and LAVIK, M. T., 1963, *Acta crystallogr.*, **16,** 1183.
JARRETT, H. S., CLOUD, W. H., BOUCHARD, R. J., BUTLER, S. R., and FREDERICK, C. G., 1968, *Phys. Rev. Lett.*, **21,** 617.

JELLINEK, F., 1962, *J. less-common Metals*, **4,** 9 ; 1963, *Arkiv Kemi*, **20,** 447.
JELLINEK, F., BRAUER, G., and MULLER, H., 1960, *Nature, Lond.*, **4710,** 376.
JOHNSTON, W. D., MILLER, R. C., and DAMON, D. H., 1965, *J. less-common Metals*, **8,** 272.
JOHNSTONE, V. A., 1956, *Prog. in Semiconductors* (ed. Gibson), **1,** 65 (London : Heywoods).
JORGENSEN, K. C., 1967, *Prog. inorg. Chem.*, **8,** 120.
JUZA, D., GIEGLING, D., and SCHÄFFER, H., 1969, *Z. anorg. allg. Chem.*, **366,** 121.
KABASHIMA, S., 1966, *J. phys. Soc. Japan*, **21,** 945.
KAMIMURA, H., and NAKAO, K. 1968, *J. phys. Soc. Jap.*, **24,** 1313 (68).
KATSUKI, S., 1969, *J. phys. Soc. Japan*, **26,** 58.
KELDYSH, L. V., and KOZLOV, A. N., 1968, *Soviet Phys. JETP*, **27,** 521.
KERSHAW, R., VLASSE, M., and WOLD, A., 1967, *Inorg. Chem.*, **6,** 1599.
KHODADAD, P., 1961, *Bull. Soc. Chim. France*, p. 133.
KITTEL, C., 1967, *Introduction to Solid State Physics*, 3rd edition (Wiley).
KJEKSHUS, A., and GRØNVOLD, F., 1959, *Acta chem. scand.*, **13,** 1767.
KJEKSHUS, A., and PEARSON, W. B., 1964, *Prog. Sol. Stat. Chem.*, **1,** 83 ; 1965, *Can. J. Phys.*, **43,** 438.
KLEMM, W., and GRIMM, L., 1942 a, *Z. Anorg. allg. Chem.*, **249,** 198 ; 1942 b, *Ibid.*, **249,** 209.
KLEMM, W., and KROSE, E., 1947, *Z. Anorg. allg. Chem.*, **253,** 209.
KNOX, R. S., 1963, *Theory of Excitons* (Academic Press).
KOGAN, V. G., and TAVGER, B. A., 1966, *Soviet Phys. Solid St.*, **8,** 808.
KOONCE, C. S., and COHEN, M. L., 1969, *Phys. Rev.*, **177,** 707.
KOONCE, C. S., COHEN, M. L., SCHOOLEY, J. F., HOSLER, W. R., and PFEIFFER, E. R., 1967, *Phys. Rev.*, **163,** 380.
KRONERT, W., and PLIETH, K., 1965, *Z. Anorg. allg. Chem.*, **336,** 207.
KÜBLER, J., 1968, *Z. Phys.*, **208,** 249.
KÜBLER, J. K., 1969, *Physics Lett.* A, **29,** 43.
LADD, L. A., and PAUL, W., 1969, *Solid St. Commun.*, **7,** 425.
LAGRENAUDIE, J., 1954, *J. de Physique*, **15,** 299.
LEE, H. N. S., MCKINZIE, H., TANNHAUSER, D. S., and WOLD, A., 1969, *J. appl. Phys.*, **40,** 602.
LEPETIT, P. A., 1965, *J. de Physique*, **26,** 175.
LEUNG, P. C., ANDERMANN, G., SPITZER, W. G., and MEAD, C. A., 1966, *J. Phys. Chem. Solids*, **27,** 849.
LEWIS, J., MACHIN, D. J., NEWNHAM, I. E., and NYHOLM, R. S., 1962, *J. chem. Soc.*, p. 2036.
LIANG, W. Y., 1967, *Physics Lett.* A, **24,** 573.
LIANG, W. Y., and CUNDY, S. L., 1969, *Phil. Mag.*, **19,** 1031.
LIANG, W. Y., and YOFFE, A. D., 1968, *Phys. Rev. Lett.*, **20,** 59.
LIN, M. S., and HARKER, H., 1968, *Solid St. Commun.*, **6,** 687.
LOHR, L. I., and MCCLURE, D. S., 1968, *J. chem. Phys.*, **49,** 3516.
MCTAGGART, F. K., and WADSLEY, A. B., 1958, *Aust. J. Chem.*, **11,** 445.
MAHAN, G. D., 1967 a, *Phys. Rev.*, **153,** 882 ; 1967 b, *Phys. Rev. Lett.*, **18,** 448.
MAKAROV, V. P., 1968, *Soviet Phys. JETP*, **27,** 173.
MALLINSON, R. B., RAYNE, J. A., and URE, R. W., 1969, *Phys. Rev.*, **175,** 1049
MANSFIELD, R., and SALAAM, S. A., 1953, *Proc. phys. Soc.* B, **66,** 377.
MARCUS, S. M., 1968, *Physics Lett.* A, **27,** 585.
MEADEN, G. T., and SZE, N. H., 1969, *Physics Lett.* A, **29,** 162.
MINOMURA, S., and DRICKAMER, H. G., 1963, *J. appl. Phys.*, **34,** 3043.
MIYAHARA, S., and TERANISHI, T., 1968, *J. appl. Phys.*, **39,** 896.
MOTT, N. F., 1967, *Adv. Phys.*, **16,** 49 ; 1968, *Rev. mod. Phys.*, **40,** 677 ; 1969, *Phil. Mag.* **20,** 1.

MULLER, A., KREBS, B., GLEMSER, O., and DIEMANN, E., 1967, *Z. Naturf.* B, **22,** 1235.
MUNSON, R. A., 1968, *Inorg. Chem.*, **7,** 389.
MUNSON, R. A., DE SORBO, W., and KOUVEL, J. S., 1967, *J. chem. Phys.*, **47,** 1769.
MUNSON, R. A., and KASPER, J. S., 1969, G.E.C. Report 69–C–047.
NEBENZAHL, I., 1969, *Phys. Rev.*, **177,** 1001.
NIKITINE, S., SCHMITT-BURKEL, J., BIELLMAN, J., and RINGEISSEN, J., 1964, *J. Phys. Chem. Solids*, **25,** 951.
OGAWA, S., 1960, *J. phys. Soc. Japan*, **15,** 1901.
PHILLIPS, J. C., 1966, *Solid St. Phys.*, **18,** 55.
PHILLIPS, J. C., and VAN VECHTEN, J. A., 1969, *Phys. Rev. Lett.*, **22,** 705.
PUOTINEN, D., and NEWNHAM, R. E., 1963, *Acta crystallogr.*, **16,** 1183.
QUINN, R. K., SIMMONS, R., and BANEWICZ, J. J., 1966, *J. phys. Chem.*, **70,** 230.
RADO, G. T., and SUHL, S., 1963/6, *Magnetism*, 4 vols. (Academic Press).
RALPH, H. I., 1965, *Solid St. Commun.*, **3,** 303.
RAMDOHR, P., 1955, *Chem. Abs.*, **49,** 13,027 f.
RAU, J. W., and KANNEWUF, C. R., 1966, *J. Phys. Chem. Solids*, **27,** 1097.
REGNAULT, F., AIGRAIN, P., DUGAS, C., and JANCOVICI, B., 1952, *C. r. hebd. Séanc. Acad. Sci., Paris*, **235,** 31.
REVOLINSKY, E., and BEERNTSEN, D., 1964, *J. appl. Phys.*, **35,** 2086 ; 1966, *J. Phys. Chem. Solids*, **27,** 523.
REVOLINSKY, E., BROWN, B. E., BEERNTSEN, D., and ARMITAGE, C. H., 1965, *J. less-common Metals*, **8,** 63.
RICE, T. M., BARKER, A. S., HALPERIN, B. J., and MCWHAN, D. B., 1969, *J. appl. Phys.*, **40,** 1337.
ROGERS, D. B., SHANNON, R. D., SLEIGHT, A. W., and GILLSON, J. L., 1969, *Inorg. Chem.*, **8,** 841.
RØST, E., and GJERTSEN, L., 1964, *Z. Anorg. allg. Chem.*, **328,** 299.
RØST, E., GJERTSEN, L., and HARALDSEN, H., 1964, *Z. Anorg. allg. Chem.*, **333,** 301.
RUDORFF, W., 1965, *Chimia*, **19,** 489.
SALAAM, S. A., 1960, *Proc. Math. Phys. Soc.* U.A.R., **24,** 41.
SALZANO, F. J., and STRONGIN, M., 1967, *Phys. Rev.*, **153,** 533.
SATO, K., ADACHI, K., OKAMOTO, T., and TATSUMOTO, E., 1969, *J. phys. Soc. Japan*, **26,** 639.
SAWAOKA, A., MINOMURA, S., and MIYAHARA, S., 1966, *J. phys. Soc. Japan*, **21,** 1017.
SCHAFER, H., 1964, *Chemical Transport Reactions* (Academic Press).
v. SCHLÄFER, H. L., and WILLE, H. W., 1967, *Z. Anorg. allg. Chem.*, **351,** 279.
v. SCHNERING, H. G., 1966, *Naturwissenschaften*, **53,** 359.
SCHOOLEY, J. F., and THURBER, W. R., 1966, *J. phys. Soc. Japan*, **21,** 639.
SELTE, K., BJERKELUND, E., and KJEKSHUS, A., 1966, *J. less-common Metals*, **11,** 14.
SELTE, K., and KJEKSHUS, A., 1964, *Acta chem. scand.*, **18,** 697 ; 1965, *Ibid.*, **19,** 258.
SENFTLE, F. E., and THORPE, A. N., 1968, *Phys. Rev.*, **175,** 1144.
SHANKS, H. R., SIDLES, P. H., and DANIELSON, G. C., 1962, Adv. in Chem. ' Non-stoichiometric Compounds ', p. 237.
SHAW, R. F., 1969, Ph.D. Thesis, Cambridge University.
SHINADA, M., and SUGANO, S., 1965, *J. phys. Soc. Japan*, **20,** 1274.
SIENKO, M. J., 1962, Adv. in Chem. ' Non-stoichiometric Compounds ', p. 224.
SILVERMAN, M. S., 1966, *Inorg. Chem.*, **5,** 2067 ; 1967, *Ibid.*, **6,** 1063.
SLATER, J. C., 1965, *Quantum Th. of Molecules and Solids*, Vol. 2 (McGraw-Hill) ; 1968, *J. appl. Phys.*, **39,** 761.

SLEIGHT, A. W., and BITHER, T. A., 1969, *J. Inorg. Chem.*, **8,** 566.
SLEIGHT, A. W., BITHER, T. A., and BIERSTEDT, P. E., 1969, *J. Phys. Chem. Solids*, **30,** 299.
SORRELL, C. A., 1968, *J. Am. ceram. Soc.*, **51,** 285.
SPARKS, J. T., and KOMOTO, T., 1963, *J. appl. Phys.*, **34** (II), 1191 ; 1968, *Rev. mod. Phys.*, **40,** 752.
SPIERING, G. A., REVOLINSKY, E., and BEERNTSEN, D. J., 1966, *J. Phys. Chem. Solids*, **27,** 535.
SPYRIDELIS, J., DELAVIGNETTE, P., and AMELINKCX, S., 1968, *Mater. Res. Bull.*, **3,** 31.
STARK, R. W., and FALICOV, L. M., 1967, *Phys. Rev. Lett.*, **19,** 795.
STRUSS, A. W., and CORBETT, J. D., 1969, *Inorg. Chem.*, **8,** 227.
SWANSON, H. E., *et al.*, 1955, N.B.S. Structure Circ. No. 529, MoS_2, **5,** 47 ; 1958, *Ibid.*, WS_2, **8,** 65.
TAKEUCHI, Y., and NOWACKI, W., 1964, *Schweiz Min. Pet. Mitt.*, **44,** 105.
TINKHAM, M., 1966, *Optical Properties of Metals and Alloys*, edited by Abeles (North-Holland), p. 431.
TOWLE, L. C., OBERBECK, V., BROWN, B. E., and STAJDOHAR, R. E., 1966, *Science, N.Y.*, **154,** 895.
TOYAZAWA, Y., and HERMANSON, J., 1968, *Phys. Rev. Lett.*, **21,** 1637.
TRACY, J. W., DUNITZ, J. D., RUNDLE, R. E., YANKEL, H. L., *et al.*, 1961, *Acta crystallogr.*, **14,** 927.
TRLIFAJ, M., 1968, *Czech. J. Phys.* B, **18,** 1576.
TUBBS, M. R., 1968, *J. Phys. Chem. Solids*, **29,** 1191.
UYEDA, R., 1968, *Acta crystallogr.*, A, **24,** 175.
UYEDA, R., and NONOYAMA, M., 1968, *J. appl. Phys.*, **7,** 200.
VAND, V., and HANOKA, J. I., 1968, *J. appl. Phys.*, **39,** 5288.
VAN MAAREN, M. H., and SCHAEFFER, G. M., 1966, *Physics Lett*, **20,** 131; 1967, *Ibid.*, **24A,** 645.
VAN MAAREN, M. H., and HARLAND, H. B., 1969, *Phys. Lett.*, **29A,** 571.
VARSANYI, F., ANDRES, K., and MAREZIO, M., 1969, *J. chem. Phys.*, **50,** 5027.
VERLEUR, A. W., BARKER, A. S., and BERGLUND, C. N., 1968, *Phys. Rev.*, **172,** 788.
VIJH, A. K., 1968, *J. Phys. Chem. Solids*, **29,** 2233 ; 1969, *J. Phys. Chem. Sol.*, **30,** 1999.
WATTS, J. A., 1966, *J. inorg. Chem.*, **5,** 281.
WESTRUM, E. F., CARLSON, H. G., GRØNVOLD, F., and KJEKSHUS, A., 1961, *J. chem. Phys.*, **35,** 1670.
WIETING, T., 1968, Ph.D. Thesis, Cambridge.
WILDERVANCK, J. C., and JELLINEK, F., 1964, *Z. Anorg. allg. Chem.*, **328,** 309.
WILSON, J. A., 1969, *J. Phys. Chem. Solids* (to be published).
WILSON, T. M., 1969, *J. appl. Phys.*, **40,** 1588.
YAMASHITA, J., ASANO, S., and WAKOH, S., 1968, *J. appl. Phys.*, **39,** 1274.
ZAHNER, J. C., and DRICKAMER, H. G., 1961, *J. chem. Phys.*, **35,** 1483.
ZAK, J., 1962, *J. Math. Phys.*, **3,** 1278.
ZEPPENFELD, K., 1968, unpublished.
ZVYAGIN, B. B., and SOBOLEVA, S. V., 1967, *Soviet Phys. crystallogr.*, **12,** 46.